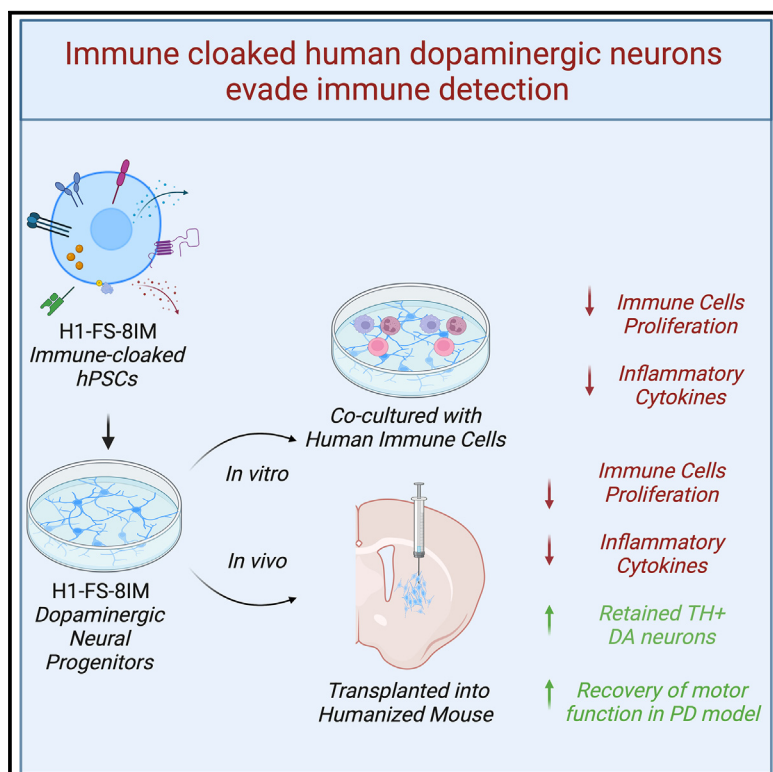


A cloaked human stem-cell-derived neural graft capable of functional integration and immune evasion in rodent models

Graphical abstract



Authors

Chiara Pavan, Kathryn C. Davidson,
Natalie Payne, ...,
Lachlan H. Thompson, Andras Nagy,
Clare L. Parish

Correspondence

chiara.pavan@florey.edu.au (C.P.),
clare.parish@unimelb.edu.au (C.L.P.)

In brief

Pavan et al. provide preclinical evidence of an engineered human “Universal” pluripotent stem cell line evading immune detection after neural engraftment in a humanized immune system mouse model and reversal of motor symptoms in Parkinsonian rats. Incorporation of a suicide gene within the universal donor cell ensures safety for cell-based therapies.

Highlights

- Cloaked human neural grafts evade immune detection in humanized mouse model
- Cloaked human neural grafts reverse motor symptoms in Parkinsonian rats
- Suicide gene incorporation into cloaked donor stem cells ensures safety

Article

A cloaked human stem-cell-derived neural graft capable of functional integration and immune evasion in rodent models

Chiara Pavan,^{1,*} Kathryn C. Davidson,^{2,7} Natalie Payne,³ Stefano Frausin,¹ Cameron P.J. Hunt,¹ Niamh Moriarty,¹ Miguel Á. Berrocal Rubio,⁴ Zahra Elahi,⁴ Andrew T. Quattrochi,¹ Kwaku Dad Abu-Bonsrah,¹ Le Wang,^{2,7} William Clow,^{2,7} Huijuan Yang,⁵ Marc Pellegrini,⁸ Christine A. Wells,⁴ Lachlan H. Thompson,^{1,6} Andras Nagy,^{3,5} and Clare L. Parish^{1,4,9,*}

¹The Florey Institute of Neuroscience and Mental Health, Melbourne, VIC, Australia

²Infectious Diseases & Immune Defence Division, Walter and Eliza Hall Institute, Melbourne, VIC, Australia

³Australian Regenerative Medicine Institute, Monash University, Clayton, VIC, Australia

⁴Department of Anatomy & Physiology, The University of Melbourne, Melbourne, VIC, Australia

⁵Lunenfeld-Tanenbaum Research Institute, Mount Sinai Hospital, Toronto, ON, Canada

⁶Faculty of Medicine and Health, School of Medical Sciences & Charles Perkins Centre, The University of Sydney, Sydney, NSW, Australia

⁷Department of Medical Biology, The University of Melbourne, Melbourne, VIC, Australia

⁸Centenary Institute of Cancer Medicine and Cell Biology, Sydney, NSW, Australia

⁹Lead contact

*Correspondence: chiara.pavan@florey.edu.au (C.P.), clare.parish@unimelb.edu.au (C.L.P.)

<https://doi.org/10.1016/j.stem.2025.03.008>

SUMMARY

Human pluripotent stem cell (hPSC)-derived therapies are a realistic possibility for numerous disorders, including Parkinson's disease. While generating replacement neurons is achievable, immunosuppressive drug challenges, to prevent rejection, remain. Here we adopted a hPSC line (termed H1-FS-8IM), engineered to overexpress 8 immunomodulatory transgenes, to enable transplant immune evasion. In co-cultures, H1-FS-8IM PSC-derived midbrain neurons evaded rejection by T lymphocytes, natural killer cells, macrophages, and dendritic cells. In humanized mice, allogeneic H1-FS-8IM neural grafts evaded rejection, while control hPSC-derived neural grafts evoked activation of human immune cells, elevated inflammatory cytokines in blood and cerebrospinal fluid, and caused spleen and lymph node enlargement. H1-FS-8IM neural grafts retained functionality, reversing motor deficits in Parkinsonian rats. Additional incorporation of a suicide gene into the H1-FS-8IM hPSC line enabled proliferative cell elimination within grafts. Findings demonstrate feasibility of generating a population-wide applicable, safe, off-the-shelf cell product, suitable for treating diseases for which cell-based therapies are a viable option.

INTRODUCTION

Cell therapy, using pluripotent stem-cell-derived cell products is a realistic prospect for many diseases including Parkinson's disease (PD). Former preclinical and clinical studies, utilizing human fetal neural tissue, have provided the necessary proof of principle for the structural and functional integration of new replacement dopamine neurons into the host brain to reverse motor symptoms in PD models and patients alike.¹ More recently, similar preclinical success has been achieved using human pluripotent stem cell (hPSC)-derived neural progenitors and led to a series of clinical trials, see Barker et al.² While these studies and trials have largely identified the working cell product and addressed necessary safety concerns, notably less is understood of the immunogenicity of these allogeneic grafts.

The central nervous system (CNS) is relatively immune privileged, with a lack of professional antigen-presenting cells

(APCs) and conventional lymphatic vessels, and evidence that allogeneic neural progenitors have low immunogenicity.³ However, the implantation procedures necessary to deliver cells into the host brain inadvertently disrupt the blood brain barrier resulting in local inflammation, evident by increase reactivity of brain's resident immune cells (microglia and astrocytes), as well as infiltrating peripheral dendritic and T cells.^{3,4} Additionally, centrally placed allogeneic antigens and immune cells can drain from the CNS via the glymphatic system and meningeal lymphatic vessels to the cervical lymph nodes and interface directly with the peripheral immune system.⁵ Here, graft antigens can be presented to naive T cells, potentially evoking a peripheral immune response that could direct activated lymphocytes to the graft site. Collectively these observations highlight that the immune response to newly implanted neurons is complex, involving many immune cell types, via both direct and indirect responses.

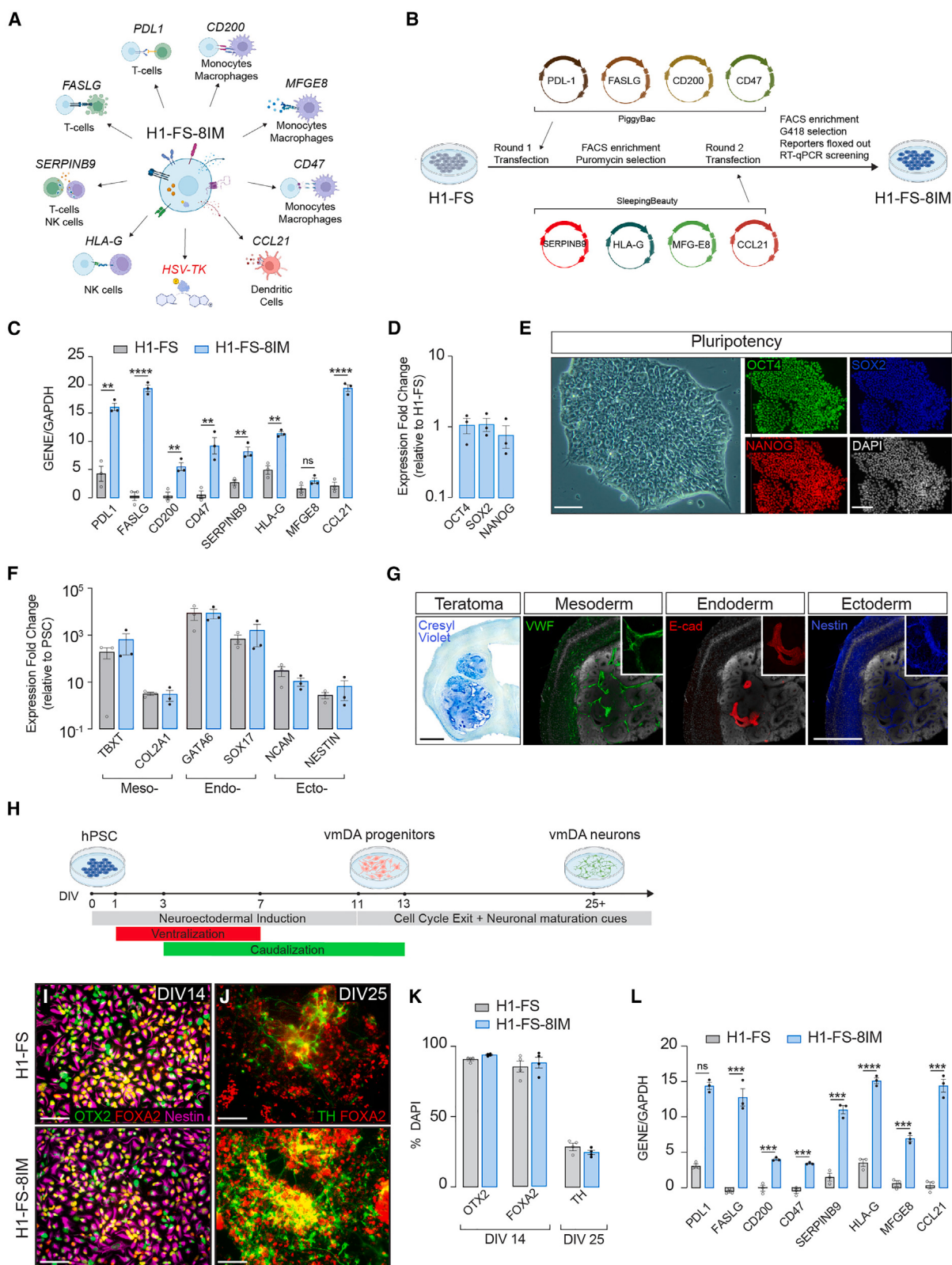


Figure 1. Generation and validation of the human H1-FS-8IM PSC and vmDA differentiation potential

(A) Schematic illustration of the 8 immunomodulatory transgenes expressed by the H1-FS-8IM hPSC line and their target immune cell, in addition to the FailSafe HSV-TK gene.

(legend continued on next page)

In an effort to address these immunological challenges, successful clinical studies in PD patients have adopted immune suppressive drug regimens to prevent neural graft rejection.³ These drugs however have significant side effects including increased susceptibility to infections, cancer risks, and a plethora of complications affecting almost every organ and culminating in shortened life expectancy.⁶ To tackle this, extensive efforts have and continue to be made to advance autologous cell grafting using patients own stem cells.⁷ In parallel have been efforts to advance and enable allogenic grafting. Presently, this requires stringent human leukocyte antigen (HLA) matching, with the proposition that “haplobanks” of hPSC lines could cover large proportions of the population. However, while the most common HLAs could be targeted, estimated at 150 iPSC lines to cover 93% of the UK and 50 lines to meet 91% of the Japanese populations, they would notably fail to serve those with less common HLAs or cover minor histocompatibility antigens,^{8,9} with evidence of residual immunological responses observed following major histocompatibility complex (MHC)-matched neural grafting in a non-human model of PD.¹⁰ More recently efforts have been made to generate donor cells that downregulate or delete highly polymorphic class I and II gene in the MHC, such as HLA-A and -B in humans, preventing T cell attack.^{11,12} While promising, these cells still present minor antigens that become the target of rejection. Consequently, several groups have further engineered cells to suppress the adaptive immune responses including, for example, the overexpression of the immunomodulatory factors PDL1, HLA-G, and/or the macrophage signal CD47 to protect the donor cells from rejection^{13–17} (for more details on the complementary approaches to generate immune-evading cells see Hotta et al.¹⁸).

In search of a strategy to produce universally tolerated cells, the field has studied exogenous cells and tissues present in nature that have developed mechanisms to hide from the immune system and avoid rejection despite expressing MHC molecules. The most emblematic cases of immune evasion are in the placenta (expressing HLA-C and HLA-G different from the mother)^{19,20} helminths,²¹ pathogens such as *M. tuberculosis*²² and some cancers.²³ In these contexts, cells “immune-cloak” themselves in an anti-inflammatory microenvironment by blocking expansion and/or lysis function of T and natural killer (NK) cells, migration and co-stimulatory activity of APCs, leukocyte-induced apoptosis, and phagocytosis. With this knowledge, we engineered a mouse²⁴ and now hPSC line to overexpress 8 immunomodulatory transgenes that have been shown to be upregulated in the placenta and cancers to evade immune

detection. These genes (*PDL1*, *CD200*, *CD47*, *HLA-G*, *FASLG*, *SERPINB9*, *CCL21*, and *MFGE8*) regulate the different classes of immune cells involved in the allogeneic immune response, referred to as “H1-8IM.” However, inducing immune tolerance raises the concern of an increased risk of tumorigenicity. Hence, the cell line was additionally engineered to express the herpes simplex virus thymidine kinase (HSV-TK) gene, transcriptionally linked to the cyclin-dependent kinase 1 gene (CDK1), to enable the FailSafe (FS) ablation of proliferative cells within the transplants following systemic administration of the activating prodrug, ganciclovir.²⁵ The resultant cell line was referred to as H1-FS-8IM.²⁴

Here, we report the evasion of H1-FS-8IM PSC-derived ventral midbrain (vm) dopaminergic (DA) neurons from immune rejection upon *in vitro* co-culturing (inclusive of T lymphocytes, NK cells, dendritic cells [DCs], and macrophages). *In vivo*, we demonstrate the ability of H1-FS-8IM PSC-derived vmDA neurons to structurally and functionally integrate in rodent PD models and reverse motor deficits, with evidence of immune evasion following implantation into a humanized immune system (HIS) mouse model.

RESULTS

Validation of H1-FS-8IM “cloaked” PSC line and its vm neural specification

The new engineered H1-FS-8IM cloaked cell line was validated for its pluripotency, maintenance of transgene overexpression, as well as neural differentiation potential. The line, designed to overexpress 8 immunomodulatory transgenes (*PDL1*, *CD200*, *CD47*, *HLA-G*, *FASLG*, *SERPINB9*, *CCL21*, and *MFGE8*) that target different classes of immune cells (T cells, NK cells, DCs, and macrophages) and carrying the FS suicide gene, HSV-TK, transcriptionally linked to the CDK1 (Figure 1A) was generated as previously described.²⁴ In brief, 2 rounds of transfections were performed using the transposon system to introduce the 8 transgenes into the H1-FS PSC line (Figure 1B). Round 1 adopted the PiggyBac transposon system to insert *PDL1*, *CD200*, *CD47*, and *FASLG* into the cells, followed by puromycin selection. A second round of targeting, using Sleeping Beauty transposons, overexpressed *HLA-G*, *SERPINB9*, *CCL21*, and *MFGE8*, with each gene linked to a reporter to enable fluorescence-activated cell sorting (FACS) selection. Finally, the 4 fluorescent reporters, used for clone selection, were floxed out of the resultant cell line, giving rise to the H1-FS-8IM F3 clone. The resultant H1-FS-8IM hPSC line was confirmed to be

(B) Targeting approach, using PiggyBac and Sleeping Beauty transposon systems, to incorporate the 8IM transgenes into the H1-FS cell line, and subsequent selection/screening to generate the H1-FS-8IM PSC line.

(C) qPCR expression of the 8 immunomodulatory genes in undifferentiated H1-FS-8IM and H1-FS hPSCs.

(D and E) (D) Pluripotency of the H1-FS-8IM PSC line was confirmed by qPCR and (E) immunocytochemistry for OCT4, SOX2, and NANOG.

(F and G) (F) Trilineage potential of the new line was confirmed by *in vitro* differentiation to meso-, endo-, and ectoderm lineages and associated gene expression, as well as (G) the ability to form teratomas.

(H) Schematic of the vmDA neural differentiation protocol.

(I–K) (I) Representative images illustrating ability of the H1-FS-8IM PSC line to differentiate into vmDA progenitors by 14 days *in vitro* (DIV) and (J) TH⁺ DA neurons by DIV25, with (K) comparable efficiency to the parental H1-FS PSC line.

(L) Retained expression of 8 immunomodulatory genes following vmDA neuronal differentiation at DIV25.

Data represent mean ± SEM. *n* = 3 independent cultures per cell line. Scale bars: (E) 100 μm, (G) 1 mm, (I) and (J) 100 μm. Abbreviations are as follows: DIV, days *in vitro*; E-cad, E-cadherin; HSV-TK, herpes simplex virus thymidine kinase; TH, tyrosine hydroxylase; vmDA, ventral midbrain dopaminergic; VWF, von Willebrand factor.

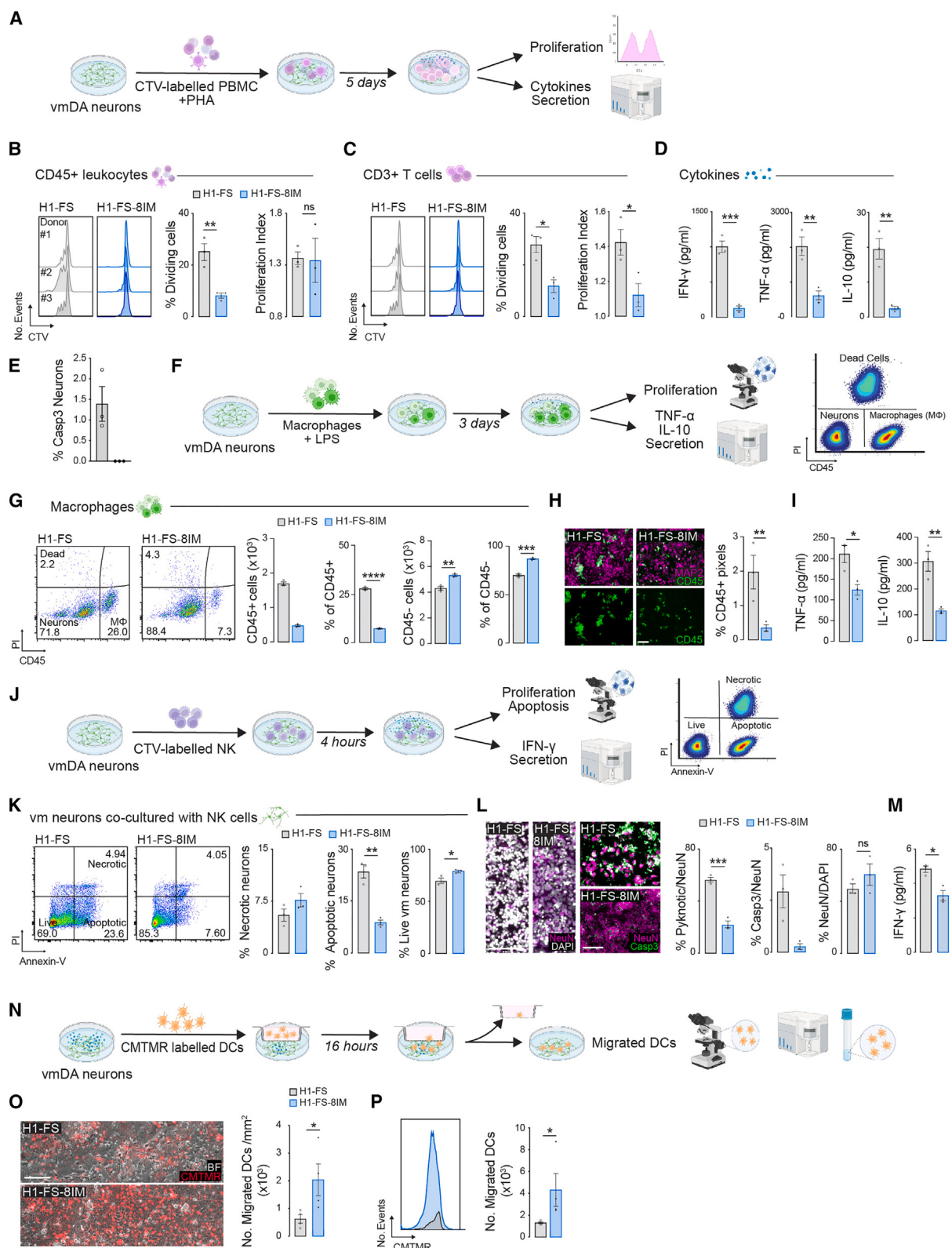


Figure 2. H1-FS-8IM-derived “cloaked” neurons are capable of evading immune detection *in vitro*

(A) Schematic overview showing co-culturing of PSC-derived vmDA neurons with CTV-labeled PBMCs to assess immune-adaptive lymphocyte proliferation and cytokine secretion.

(legend continued on next page)

karyotypically normal (Figure S1A), and quantitative PCR (qPCR) confirmed elevated expression of the 8 immunomodulatory genes, compared with the H1-FS PSC line (Figure 1C). Comparable expression of pluripotency genes (*OCT4*, *SOX2*, and *NANOG*) was demonstrated between the two hPSC lines (Figure 1D) and validated by the high proportion (>99%) of immuno-label cells in undifferentiated H1-FS-8IM PSC cultures (Figures 1E, S1B and S1C).

Multi-lineage potential of H1-FS-8IM hPSC line was confirmed using the STEMdiff Trilineage Differentiation Kit (StemCell Technologies) and RT-qPCR for lineage-specific targeted genes (mesoderm: TBXT/brachyury and COL2A1/collagen; endoderm: GATA6 and SOX17; ectoderm: neural cell adhesion molecule [NCAM] and Nestin) (Figures 1F and S1D). Presence of mesoderm (Von Willebrand factor [vWF]), endoderm (E-cadherin [E-cad]), and ectoderm (Nestin)-derived cell populations within teratomas, 4 weeks after intracerebral delivery of undifferentiated H1-FS-8IM PSCs into athymic mice (Figure 1G) additionally confirmed the trilineage potential of the cell line.

In preparation for neural grafting and assessment of the universal cell to evade detection in a Parkinsonian disease model, the H1-FS-8IM PSC line was assessed for its ability to differentiate into ventral midbrain dopaminergic (vmDA) neural progenitors, suitable for cell replacement, using our established protocol (Figure 1H). H1-FS-8IM PSCs competently differentiated into vmDA progenitors, verified by the high proportion (>90%) of OTX2, FOXA2, and Nestin immunoreactive cells at 14 days of differentiation (DIV14) (Figures 1I and 1K) and by DIV25 >25% tyrosine hydroxylase (TH⁺) neurons, noting TH is the rate limiting enzyme in dopamine synthesis and marker of dopamine neurons (Figures 1J and 1K) comparable and as previously reported for

the H1-FS PSC line.²⁶ Importantly, upon terminal differentiation, H1-FS-8IM postmitotic neurons retained overexpression of the 8 immunomodulatory genes, at levels orders of magnitude than H1-FS-derived neurons (Figure 1L).

H1-FS-8IM-derived neurons are capable of evading immune detection *in vitro*

The ability of H1-FS-8IM-derived neurons to evade detection by immune cells was initially tested *in vitro*. Day 19 H1-FS and H1-FS-8IM vmDA progenitors were co-cultured with cell trace violet (CTV)-labeled peripheral blood mononuclear cells (PBMCs) derived from 3 blood donors and treated with phytohaemagglutinin (PHA) to stimulate a lymphocyte response. After 5 days of co-culture, supernatant was collected and analyzed for proliferating CD45⁺ immune cells (based on CTV dilution) and secreted cytokine levels (Figure 2A). CD45⁺ cells were FACS gated as illustrated in Figure S2A. All 3 PBMC blood donors showed significantly reduced proportion of dividing cells when co-cultured with H1-FS-8IM neurons, compared with H1-FS neurons while the proliferation index (average number of divisions that excludes the non-dividing cell population) remained unchanged (Figure 2B) reflective of a suppressed immune response evoked by the immune-cloaked neurons.

Closer examination, selectively of the CD3⁺ population (representative FACS gating, Figure S2A), revealed that the majority of the immune response to the H1-FS neurons was T cell mediated, with a significant increase in the proportion of dividing cells (H1-FS: 27.91 ± 3.10; H1-FS-8IM: 11.74 ± 2.45, $p = 0.0149$) and T cell proliferation index (H1-FS: 1.42 ± 0.074; H1-FS-8IM: 1.12 ± 0.07, $p = 0.0376$) (Figure 2C). During acute allograft rejection, cytokines interferon-gamma (IFN- γ), tumor necrosis factor

(B) Representative FACS plots from 3 PBMC donors showing CTV-detected PBMC proliferative cycles (peaks) when cultured with HLA-incompatible H1-FS neurons, but no proliferation in the presence of cloaked H1-FS-8IM neurons, and quantification of the proportion of proliferating CD45⁺ lymphocytes and proliferation index (i.e., cells undergoing >1 division).

(C) Representative FACS plots of CD3⁺ gated cells, illustrating the T lymphocyte response to the H1-FS, but not cloaked H1-FS-8IM neurons, the quantitative proportion of dividing T cells and their proliferation index.

(D) Quantification of cytokine levels within supernatant from co-cultures of donor PBMCs with H1-FS-derived neurons revealed significantly elevated levels, compared with H1-FS-8IM-derived neurons.

(E) Reflective of the elevated T cell response, apoptotic neurons (Casp3⁺/NeuN⁺) were only observed in H1-FS co-cultures.

(F) Overview of H1-FS or H1-FS-8IM neurons co-cultured with LPS-treated macrophages and their quantitative assessment after 3 days.

(G) Representative FACS plots and quantification of the total number and % CD45⁺ macrophages revealed a significant reduction in the macrophages population following co-culture with cloaked H1-FS-8IM neurons. Reduced %CD45⁻ cells (i.e., neurons) within H1-FS co-cultures reflected the proportionate increase in CD45⁺ macrophages.

(H) Representative photomicrographs and quantification showing no difference in the proportion of MAP2⁺ neurons (magenta), yet decrease in CD45⁺ macrophages (green) in H1-FS-8IM, compared with H1-FS co-cultures.

(I) Quantification of macrophage-secreted cytokines confirmed an elevated immune response in H1-FS, compared with H1-FS-8IM co-cultures.

(J) H1-FS and H1-FS-8IM neurons were co-cultured with CTV-labeled NK cells and assessed for proliferation, survival, and IFN- γ secretion.

(K) Example FACS plots illustrating the proportion of apoptotic and necrotic death within the CTV⁻ (i.e., neuronal) population. Quantification revealed no significant difference in necrotic cell death but a significant reduction in apoptotic death of H1-FS-8IM-derived neurons, compared with H1-FS neurons, and consequently a proportionate increase in live neurons.

(L) Representative images and quantification, showing increased DAPI-labeled pyknotic nuclei and Casp3⁺ apoptotic cells in H1-FS, compared with H1-FS-8IM-derived neuronal cultures.

(M) Quantification of the major NK secreted cytokine, IFN- γ , within the supernatant.

(N) Schematic illustration showing the transwell co-culture of vmDA neurons (seeded onto the plastic) and CMTMR-labeled dendritic cells (DCs) (plated into the transwell), to track DC migration.

(O) Sample photomicrographs and quantification revealed an increased density of CMTMR-labeled DCs when co-cultured on H1-FS-8IM neurons.

(P) Representative FACS plot and quantitative confirmation of increased migrated DC cells in the lower transwell chamber from H1-FS-8IM co-cultures.

Data represent mean ± SEM, Mann-Whitney U test or Student's *t* test. (B)–(E) $n = 3$ independent cultures/experiment, repeated for 3 PMBC donors. (F)–(P) $n = 3$ –4 independent cultures/experiment. * $p < 0.05$; ** $p < 0.01$; *** $p < 0.001$, **** $p < 0.0001$. Scale bars: (H), (L), and (O) 50 μ m.

Abbreviations are as follows: Casp3, cleaved caspase-3; CMTMR, CellTracker orange; CTV, cell trace violet; DC, dendritic cells; LPS, lipopolysaccharides; MAP2, microtubule-associated protein 2; NeuN, neuronal nuclear protein; NK, natural killer; PHA, phytohaemagglutinin; vmDA, ventral midbrain dopaminergic.

alpha (TNF- α) and interleukin-10 (IL-10) are upregulated.²⁷ Reflective of the suppressed immune cell proliferation in H1-FS-8IM-derived neurons co-cultured with PBMCs, a significant reduction in all 3 cytokines was observed (Figure 2D). Reflective of the elevated T cell response, apoptotic neurons (Casp3 $^+$ NeuN $^+$) were only observed in uncloaked H1-FS co-cultures and not H1-FS-8IM cultures (Figure 2E).

While T lymphocytes in the CNS compartment (meninges) carry out constant immune surveillance,²⁸ other immune cell types can be activated in the periphery, in response to inflammatory signals, and infiltrate the brain particularly after cell transplantation where the blood brain barrier is disrupted.³ We therefore assessed the ability of cloaked H1-FS-8IM neurons to evade other immune populations involved in graft rejection. To assess the ability of the H1-FS-8IM immune-cloaked neurons, overexpressing CD47, CD200, and MFG-E8 transgenes that target inhibition of phagocytosis by monocytes/macrophages,^{29–31} H1-FS or H1-FS-8IM derived vmDA neurons were co-cultured with unstimulated (Figures S2D–S2H) and lipopolysaccharide (LPS)-stimulated (Figures 2F–2I) macrophages derived from hPSCs for 3 days. Confirmation of the identity of the hPSC-derived macrophages was benchmarked to PBMC-derived macrophages (showing comparable CD14, CD16, and CD11b expression), co-expression of the microglia/macrophage-specific calcium-binding protein Iba1 with CD45 $^+$, and FACS-gated isolation of cells expressing CD34 (a marker shared with hemogenic endothelium and early hematopoietic stem cells [HSCs]) with CSF1R (myeloid specific marker) within a population of CD45 $^+$ cells (Figure S2B) as previously described.^{32,33}

Enzymatic dissociation (to collect both adherent and floating macrophages) and FACS gating of the CD45 $^+$ macrophages (Figure S2C) showed an increase in the number and proportion of macrophages in H1-FS, compared with H1-FS-8IM neuron co-cultures (Figure 2G). A significant decrease in the number and proportion of CD45 $^+$ cells was observed in the H1-FS cultures, reflective of the relative increase in proportion of CD45 $^+$ cells. As there was no change in total propidium iodide (PI)-labeled dead cells observed between H1-FS and H1-FS-8IM cultures, accounting for <5% total cells in both cultures (Figure 2G), the decrease in neuronal number in H1-FS may indicate increased neuronal death and phagocytosis of dead neurons by macrophages in the H1-FS cultures. In agreement, immunocytochemical staining for CD45 $^+$ macrophages and MAP2 $^+$ neurons revealed a significant increase in activated macrophages (displaying a classical “fried-egg” morphology) in H1-FS cultures, quantified as the proportion of CD45 $^+$ immunoreactive pixels (Figure 2H). Closer examination of macrophages + H1-FS neuron co-cultures revealed neuronal phagocytosis, evident by the significant increase CD45 $^+$ macrophages (Figure S2G) and those engulfing MAP2 $^+$ neurons, compared with cloaked co-cultures (Figure S2I). In response to inflammatory stimuli (e.g., LPS), macrophages are the main source of circulating TNF- α , promoting a pro-inflammatory response, which is capable of recruiting other immune cell types. Additionally IL-10, also secreted by macrophages, is both a pro- and anti-inflammatory cytokine, with a major role in the first phases of an immune response.²⁷ In line with the increase in macrophages in uncloaked H1-FS-derived neuronal co-cultures, a significant increase in both cytokines was observed (TNF- α levels; H1-FS:

211.01 \pm 20.56 pg/mL; H1-FS-8IM: 124.40 \pm 12.60 pg/mL, p = 0.0229; IL-10 levels; H1-FS: 306.9 \pm 38.07 pg/mL; H1-FS-8IM: 115.3 \pm 7.986 pg/mL, p = 0.0079) (Figure 2I). Note, similar elevated macrophage proliferation and cytokine responses were observed when unstimulated macrophage (i.e., –LPS treatment) were co-cultured with uncloaked H1-FS vmDA neurons (Figures S2D–S2H).

Following immune stimulation, serine proteinase inhibitor B9 (Serpin B9) helps to protect cells by inhibiting granzyme B (a protease released by NK cells that induces apoptosis in target cells), while HLA-G suppresses NK cell activity through inhibitory receptor engagement.^{34,35} To assess the efficiency of SERPINB9 and HLA-G transgene overexpression in cloaked neurons to evade the NK cell response, H1-FS-8IM (and H1-FS) derived neurons were co-cultured with NK-92 cells (a NK cell line derived from PBMC) and subsequently screened for cell death and cytokine release (Figure 2J). NK-92 cells were labeled with CTV to enable subsequent discrimination of the neurons (CTV $^+$) from the NK cells (CTV $^+$) (representative FACS gating, Figure S3A). As NK cells can exert cytotoxicity, the neurons were labeled with PI and Annexin V to distinguish necrotic cell death (PI $^+$ AnnexinV $^+$ cells) from apoptotic (PI $^-$ AnnexinV $^+$) (Figures 2J–2K).

Reflective of immune evasion, H1-FS-8IM hPSC-derived vmDA neurons showed a significant decrease in PI $^-$ AnnexinV $^+$ apoptotic cells, compared with H1-FS neurons (H1-FS-8IM: 8.82 \pm 0.80; H1-FS: 23.49 \pm 1.88, p = 0.002), and resulted in a subtle but significant increase in the proportion of viable vmDA neurons (Figure 2K). The NK cells (following co-culture with H1-FS-8IM neurons) similarly showed a decreased proportion of PI $^-$ AnnexinV $^+$ apoptotic cells (Figure S3B). No difference was observed in the proportion of PI $^+$ AnnexinV $^+$ necrotic neurons between the two hPSC lines. Reflective of reduced apoptosis in cloaked neuronal cultures, a reduction in pyknotic nuclei and Casp3 $^+$ NeuN $^+$ cells were observed (Figure 2L) and similarly within the CD45 $^+$ NK cell population (Figure S3C). Indicative of IFN- γ being one of most powerful effector cytokine secreted by NK cells during the earliest phases of an immune response,³⁶ a significant increase was observed in H1-FS, compared with H1-FS-8IM neuronal cultures (Figure 2M). These findings were validated using primary NK cells isolated from PBMCs (Figure S3D), where Calcein-AM labeling of the H1-FS neurons were shown to be attacked by the NK cells—evident by the reduction in Calcein-AM-labeled neurons and elevated levels of lactate dehydrogenase (LDH) within the media (Figures S3E and S3F).

CCL21 encodes a chemokine expressed in the lymph nodes that recruits activated DCs to prime cells of the adaptive immune system.³⁷ Overexpression of CCL21 by cloaked cells is likely to disrupt the ability of local DCs to migrate to the lymph nodes and activate adaptive immunity. This immune escape mechanism is seen in some cancers where expression impairs DC migration and protects cancer from immune attack.³⁸ Commensurate with transgene overexpression, protein analysis confirmed elevated CCL21 in the media collected from undifferentiated H1-FS-8IM hPSC and vmDA progenitors (Figure S4A). To confirm the immune escape mechanism of the cloaked neurons, hPSC-derived DCs (CD1c $^+$, CD11c $^+$, representative FACS gating shown in Figure S4B) were pre-labeled with CellTracker Orange (CMTMR) dye and placed on the upper chamber of a

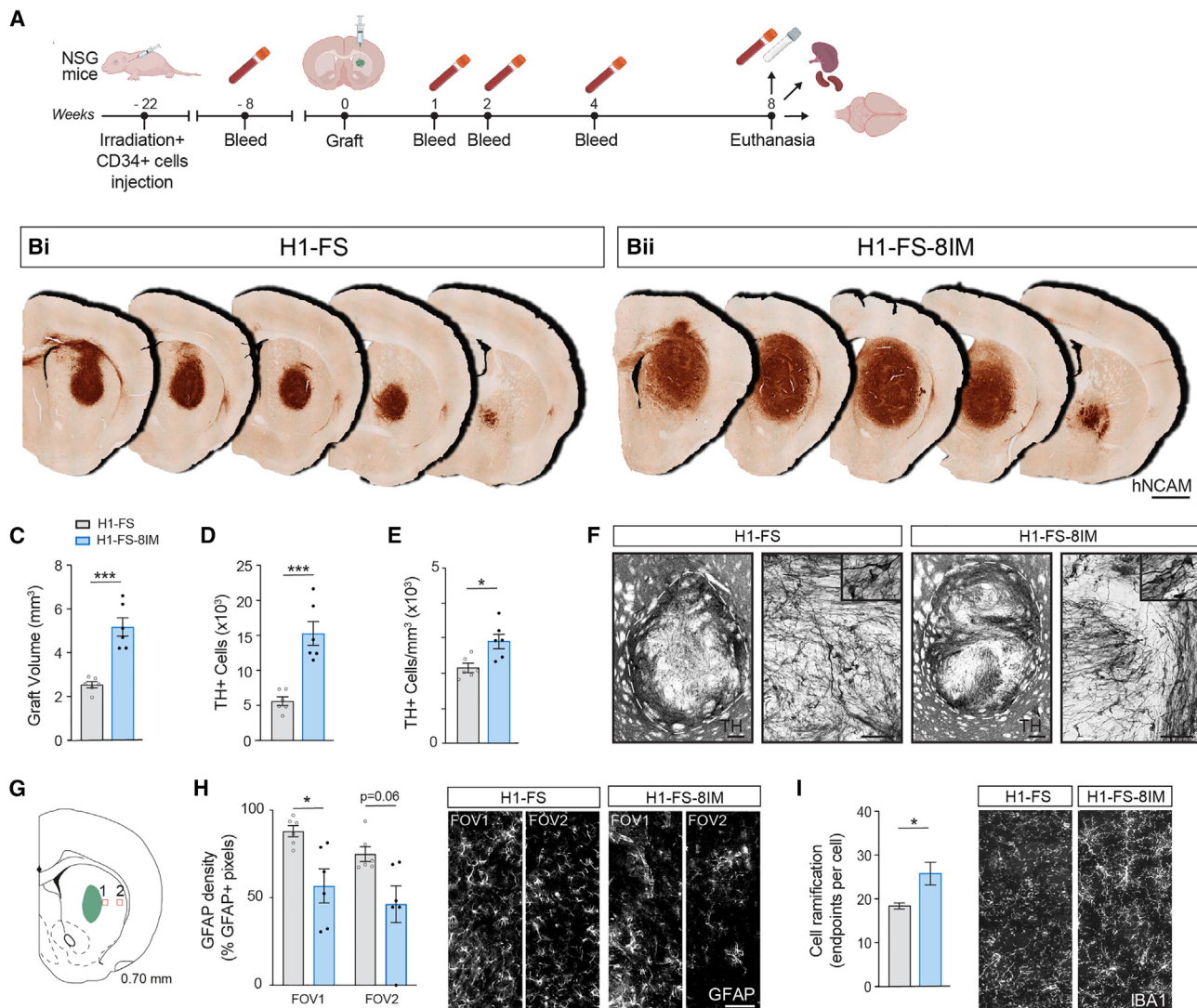


Figure 3. Cloaked vmDA progenitors show improved graft survival and evasion of resident immune cells in the brain

(A) Schematic showing generation of the NSG humanized mice (via irradiation and human CD34⁺ cord blood cells delivery), validation of humanization via intermittent bleeds, transplantation, and post-mortem assessments.

(B) Representative micrographs showing a H1-FS PSC-derived (i) and larger H1-FS-8IM-derived neural graft (ii).

(C–E) Cloaked neural grafts were significantly larger and (D) contained more TH⁺ DA neurons, (E) and TH⁺ cell density.

(F) Representative images of TH⁺ neurons within the grafts at 8 weeks post-transplantation.

(G) Density of resident astrocytes and microglia were assessed at the graft-host border (1, FOV1, field of view) and 500 μm distal to the graft core (2; FOV2), as depicted in the schematic.

(H and I) Quantitative assessment revealed decreased host-derived GFAP⁺ reactive astrocytes density in animals receiving cloaked, compared with uncloaked, neural grafts. While no change in density of Iba1⁺ microglia was observed (not shown), host Iba1⁺ microglia showed significantly fewer ramifications and greater amoeboid-like morphology in animals receiving uncloaked H1-FS neural grafts.

Data represents mean ± SEM, Mann-Whitney U test or Student's t test. (B)–(I) n = 6 grafts/group. *p < 0.05; **p < 0.01, ***p < 0.001. Scale bars: (B) 1 mm, (H), and (I) 100 μm.

Abbreviations are as follows: GFAP, glial fibrillary acidic protein; hNCAM, human neural cell adhesion molecule; Iba1, ionized calcium-binding adaptor molecule 1; TH, tyrosine hydroxylase.

transwell with either H1-FS-8IM- or H1-FS-derived vmDA progenitors in the lower chamber, as depicted in Figure 2N. In response to elevated CCL21, secreted from the H1-FS-8IM vmDA progenitors, DCs showed increased migration, evident by the increase in CMTMR-labeled DCs within the lower chamber of the well containing the neural progenitors, assessed by

fluorescence microscopy (Figure 2O) and flow cytometry (Figure 2P, representative FACS gating Figure S4C). In summary, H1-FS-8IM-derived neural progenitors demonstrated the capability to evade multiple immune cell populations involved in graft rejection, namely T lymphocytes, NK cells, macrophages, and DCs *in vitro*.

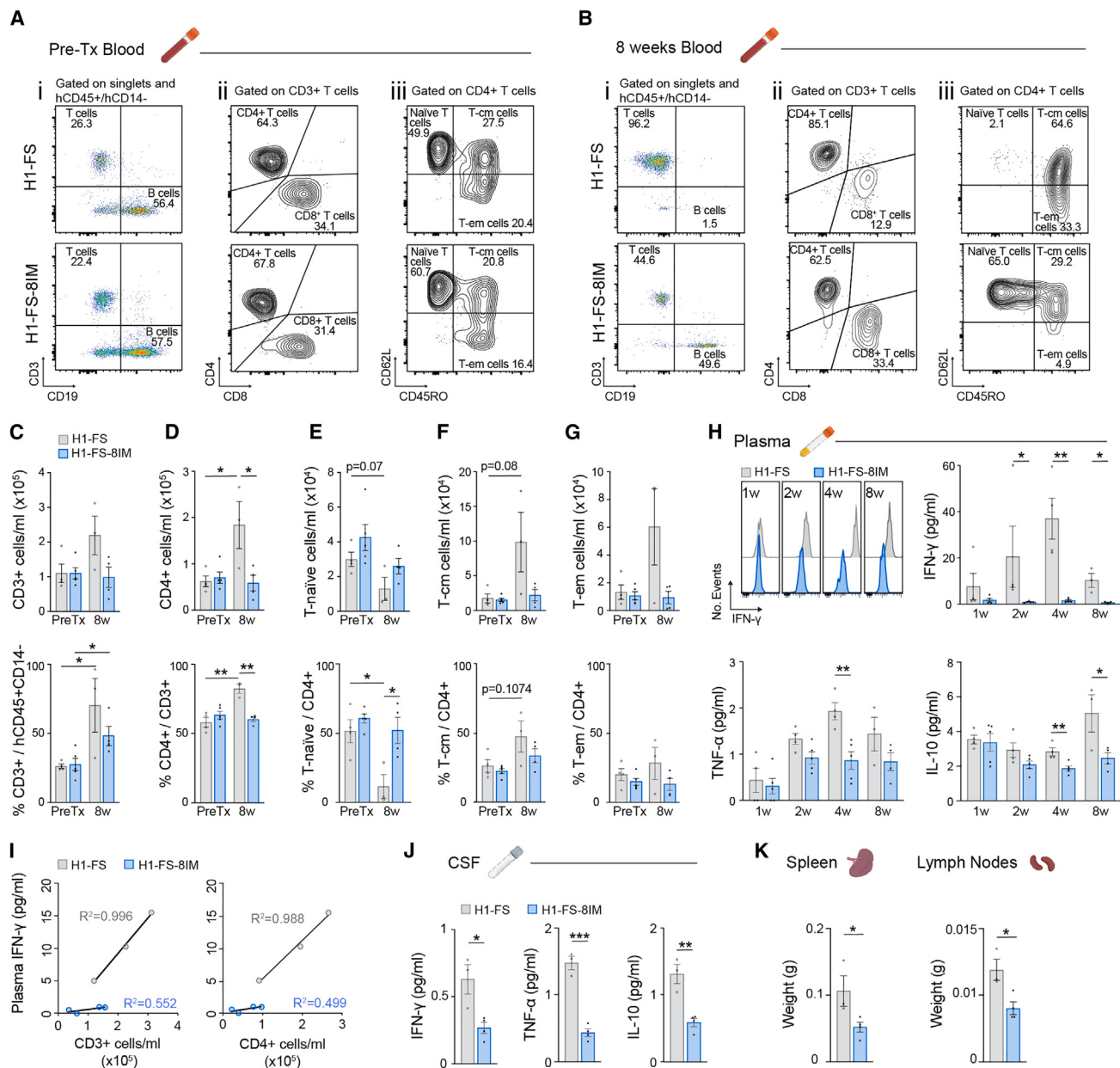


Figure 4. Human uncloaked PSC-derived vmDA progenitor grafts, but not those derived from cloaked PSCs, induce a cytotoxic T lymphocyte response and elevated cytokines in a humanized mouse model

(A and B) (A) Representative FACS plots of mouse blood samples illustrating gating of B and T lymphocyte populations before (pre-Tx) and (B) after transplantation (8 weeks post-Tx) of H1-FS- and H1-FS-8IM hPSC-derived vmDA neurons into mice humanized with CD34⁺ cord blood cells (HIS mice).

(C and D) Quantification of the number/mL and proportion of CD3⁺ total T cells and (D) CD4⁺ T helper cells, showing an elevated immune response after transplantation of H1-FS (gray bars), but not H1-FS-8IM (blue bars) PSC-derived neural grafts.

(E) Reflective of T cells activation, the proportion of naive T cells was significantly decreased after the transplantation of uncloaked (H1-FS PSC derived) neural grafts yet remained unchanged in animals receiving cloaked grafts.

(F and G) (F) Quantification of CD4⁺ memory T cells (T-cm) and (G) effector T cells (T-em), both derived from naive T cells and retaining short- and long-term roles in the immune response, respectively, showed elevated numbers in circulation in animals receiving uncloaked, but not cloaked, hPSC-derived neural grafts.

(H) Representative FACS plots showing IFN- γ plasma levels in HIS mice receiving uncloaked (gray) and cloaked (blue) neural transplants. Elevated IFN- γ , TNF- α , and IL-10 blood plasma levels post-transplantation in animals receiving cloaked, but not uncloaked neural grafts.

(I) Regression analysis illustrating the positive correlation between circulating T cell numbers (CD3⁺ and CD4⁺) and IFN- γ levels, reflective of a T cell-specific immune response, in animals receiving uncloaked, but not cloaked, H1-FS-8IM neural grafts.

(J) Similar to blood plasma, levels of IFN- γ , TNF- α , and IL-10 were significantly elevated in the CSF of HIS mice 8 weeks post-transplantation with uncloaked neural progenitors.

(legend continued on next page)

Cloaked H1-FS-8IM-derived neural grafts show superior engraftment, with evidence of immune evasion in a humanized mouse model

To demonstrate the ability of H1-FS-8IM cloaked neural grafts to evade immune detection, differentiated neural progenitors were implanted into adult mice with varying immune competency (**Figures 3A** and **S5A**). In immune-competent Swiss mice, at 8 weeks post-implantation, there was no evidence of surviving H1-FS and H1-FS-8IM hPSC-derived neural grafts, confirmed by a lack of human-specific NCAM (hNCAM) staining (**Figures S5B** and **S5C**). In contrast, neural grafts, derived from either hPSC line, showed engraftment in athymic immune-compromised nude mice, with comparable graft size and complement of TH⁺ DA neurons (**Figures S5B–S5E**). In HIS mice, generated by reconstituting immunodeficient non-obese diabetic (NOD)-severe combined immunodeficiency (*scid*) IL2Rg^{null} (NOD scid gamma, NSG) neonates with allogeneic (**Figure S1E**) human umbilical cord-derived CD34⁺ hematopoietic cord blood stem cells (**Figure 3A**), H1-FS-8IM hPSC-derived neural grafts were notably larger than H1-FS neural grafts (H1-FS: $2.54 \pm 0.14 \text{ mm}^3$; H1-FS-8IM: $5.18 \pm 0.42 \text{ mm}^3$, $p = 0.0001$, **Figures 3B** and **3C**). TH⁺ immunolabeling revealed a significant increase in dopamine neurons within the H1-FS-8IM-derived grafts (H1-FS: $5.39 \times 10^3 \pm 0.60 \times 10^3$; H1-FS-8IM: $14.66 \times 10^3 \pm 1.64 \times 10^3$, $p = 0.0003$, **Figure 3D**), reflective of graft volume, and increased DA cell density (H1-FS: $2.10 \times 10^3 \pm 0.16 \times 10^3$; H1-FS-8IM: $2.83 \times 10^3 \pm 0.21 \times 10^3$, $p = 0.0193$, **Figures 3E** and **3F**). Assessment of the resident inflammatory cells in the brain at the graft-host interface (field of view 1 [FOV1]), as well as distal to the graft core, (FOV2, **Figure 3G**) revealed a significant reduction in GFAP⁺ reactive astrocytes in mice receiving H1-FS-8IM, compared with H1-FS hPSC-derived neural grafts (**Figure 3H**). No change in the number of Iba1⁺ microglia was observed (data not shown); however, morphological assessment revealed significantly reduced ramifications and increasing amoeboid morphology, indicative of reactive microglia, surrounding the uncloaked (H1-FS-derived) neural grafts (**Figure 3I**).

More detailed examination of the immune-evasive capabilities of the H1-FS-8IM neural graft was assessed in HIS grafted mice by screening blood (at various intervals before and after transplantation), cerebrospinal fluid (CSF), and lymph tissues, as illustrated in **Figure 3A**. Focusing on circulating human lymphocytes (i.e., human CD45⁺CD14⁻, **Figure S6A**) in the blood, all HIS mice assigned to received neural grafts showed comparable level of circulating human CD45⁺ immune cells, CD3⁺, CD4⁺, and CD8⁺ T cells, CD19⁺ B cells and CD14⁺ monocytes prior to transplantation (**Figures 4A**, **4C**, **4D** and **S6B–S6J**). Reflective of an adaptive immune activated response, transplantation of uncloaked H1-FS-derived neural progenitors resulted in a 2-fold increase in the number and proportion of circulating CD3⁺ T lymphocytes at 8 weeks after transplantation (**Figures 4Bi** and **4C**). More targeted assessment revealed a significant (3-fold) increase in CD4⁺ T helper cells (**Figures 4Bii** and **4D**) the subpop-

ulation of T cells responsible for driving the immune response, with a reduction in unactivated/resting/quiescent CD62L⁺ CD45RO⁻ naive T cells and a trend of an increase in both activated CD62L⁺CD45RO⁺ central memory T cells and CD62L⁻CD45RO⁺ effector memory T cells (**Figures 4Biii** and **4E–4G**). In contrast, no elevation in the total number or proportion of T cells (inclusive of T helper, T effector, and T memory cells) was observed in mice receiving cloaked H1-FS-8IM grafts (**Figures 4Biii** and **4G**) rather the majority (52%) of circulating T helper cells were CD62L⁺ CD45RO⁻ naive T cells (**Figure 4E**).

Reflective of the proliferative T cell adaptive immune response to the uncloaked H1-FS-derived neural graft, FACS analysis showed a significant increase in plasma levels of IFN- γ , TNF- α , and IL-10, compared with animals receiving H1-FS-8IM neural grafts (**Figure 4H**). Of note, cytokine levels remained not significantly different in HIS mice prior to or at 1 week after transplantation of H1-FS-8IM neural progenitors (IFN- γ before transplantation: 4.2 ± 2.1 , after: 1.68 ± 1.1 ; TNF- α before transplantation: 0.94 ± 0.42 , after: 0.60 ± 0.22 ; IL-10 before transplantation: 2.02 ± 0.49 , after: 3.37 ± 0.82). In mice receiving uncloaked neural grafts, the peak of IFN- γ , and TNF- α levels detected in the plasma was observed at 4, diminishing by 8 weeks post-transplantation, correlating with the diminishing humanization of the mice over time (**Figure S6B**). Regression analysis highlighted the strong correlation between plasma IFN- γ levels and total CD3⁺ T cells ($R^2 = 0.996$) as well as CD4⁺ T helper cells ($R^2 = 0.988$) in mice receiving uncloaked neural grafts, while no such relationship was observed in animals receiving neural grafts derived from H1-FS-8IM PSCs ($R^2 = 0.552$ and $R^2 = 0.499$, respectively), indicating that T cells were the main population responsible for IFN- γ production (**Figure 4I**). Terminal collection of CSF similarly showed significant higher levels of the 3 cytokines in mice with uncloaked (H1-FS PSC-derived) neural grafts (**Figure 4J**).

As a final assessment of the immune response, spleen and cervical lymph nodes were collected at 8 weeks post-transplantation. Both organs were significantly enlarged in animals receiving uncloaked neural grafts (**Figure 4K**). FACS assessment of T lymphocyte subpopulations revealed a significant increase in CD3⁺ T lymphocytes proportion within the spleen of mice receiving uncloaked H1-FS grafts (H1-FS: $77.80\% \pm 9.41\%$, H1-FS-8IM: $49.10\% \pm 6.64\%$; $p = 0.049$), with notable trends of elevated CD4⁺ T helper (4.7-fold increase, $p = 0.114$ for CD4⁺ cells/mL; 1.65-fold increase, $p = 0.057$ for % CD4⁺/CD3⁺) and a reciprocal reduction in CD62L⁺/CD45RO⁻ naive T cells (2.17-fold decrease, $p = 0.114$ for cells/mL; 4.48-fold decrease, $p = 0.114$ for % T naive/CD4⁺) (**Figures S6K** and **S6L**).

Activation of a suicide gene within the H1-FS-8IM cells ensures the safety for adopting immune cloaking strategies *in vivo*

A primary concern of a cell capable of evading immune detection is the risk of malignancy. The inclusion of the previously reported FS

(K) Spleen and lymph nodes, reservoirs of immune cells, increased in weight in HIS mice receiving uncloaked H1-FS, but not H1-FS-8IM neural grafts, reflective of antigen presentation and an adaptive immune response.

Data represent mean \pm SEM, Mann-Whitney U test or Student's t test. (B)–(D) $n = 4$ –5 grafted animals/group, * $p < 0.05$; ** $p < 0.01$; *** $p < 0.001$.

Abbreviations are as follows: 8w, 8 weeks; CSF, cerebrospinal fluid; pre-Tx, pre-transplantation; post-Tx, post-transplantation; T-cm, T central memory cells; T-em, T effector memory cells.

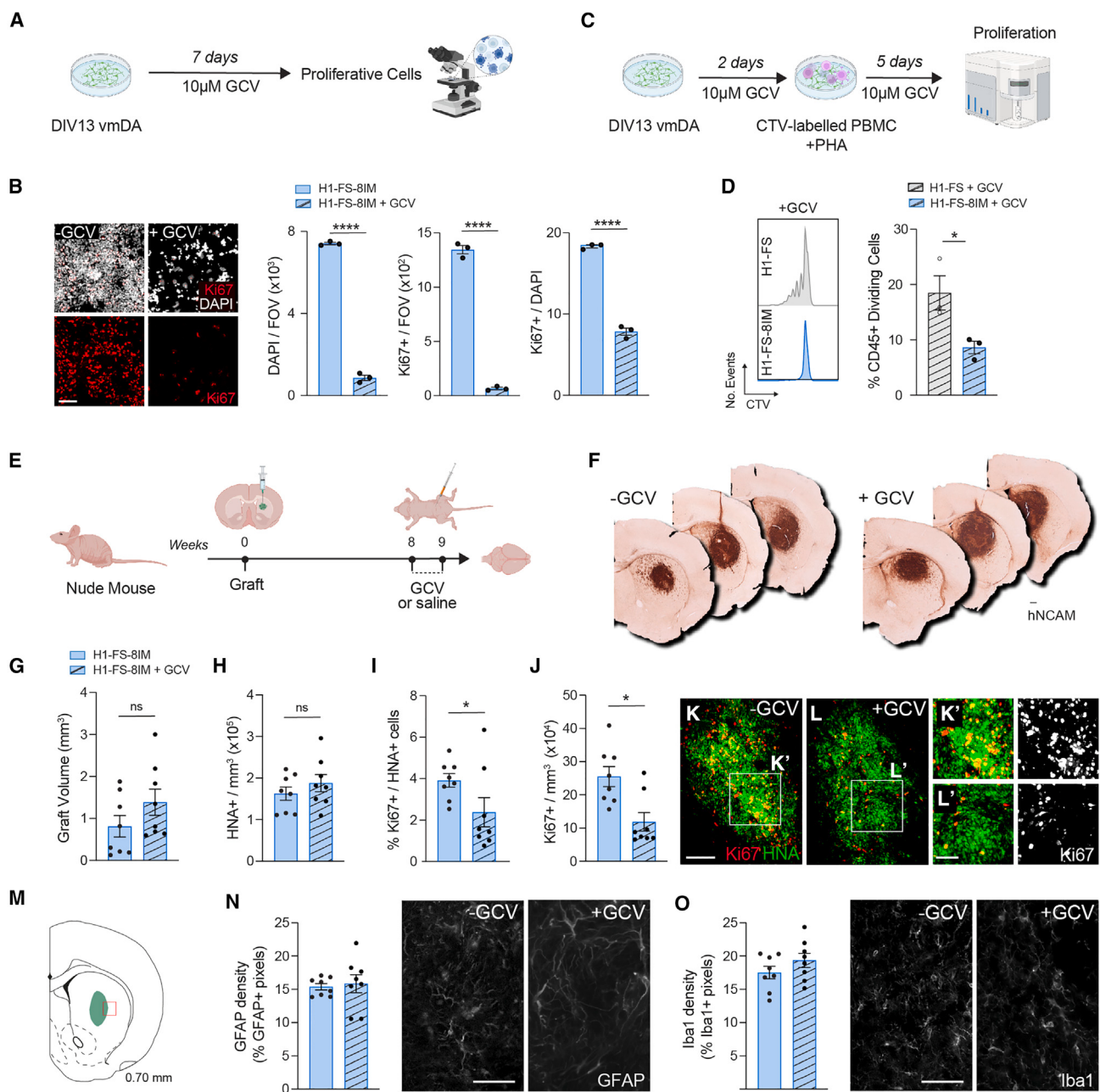


Figure 5. The suicide gene within the H1-FS-8IM cloaked PSC cell line remains functional and able to ablate proliferative progenitors *in vitro* and *in vivo*.

- (A) Schematic overview showing vmDA progenitor cultures and the ganciclovir (GCV) activation of the HSV-TK suicide gene.
- (B) Representative images and quantification of total (DAPI) and proliferating (Ki67⁺) cells within day 20 vmDA cultures, following treatment with GCV.
- (C) Schematic overview of co-culturing of PSC-derived vmDA neurons (treated with GCV) together with CTV-labeled PBMCs aimed at assessing the impact of suicide gene activation on immune cell proliferation.
- (D) Representative FACS plots and quantification of CTV-labeled CD45⁺ lymphocytes showing that GCV treatment does not alter the immune evasive properties of H1-FS-8IM-derived neurons.
- (E) Schematic time course of H1-FS-8IM neural progenitor transplantation and GCV treatment in athymic nude mice.
- (F) Representative images showing a H1-FS-8IM PSC-derived vmDA progenitor graft (\pm GCV treatment) in immunodeficient mice.
- (G–J) (G) Quantification of graft volume, (H) density of human nuclear antigen (HNA⁺) cells, (I) Ki67 proportion, and (J) density of Ki67⁺ proliferating cells within GCV-treated and -untreated grafts.
- (K and L) Representative images depicting fewer Ki67⁺ cells in graft from animal treated with GCV, compared with saline.

(legend continued on next page)

suicide gene (HSV-TK, transcriptionally linked to the cell-cycle essential gene cyclin D1, CDK1) into the donor hPSC enables selective ablation of proliferative cells,²⁵ including within neural grafts.²⁶ To demonstrate that the cloaking system did not impact the efficacy of the suicide gene system, H1-FS-8IM hPSC-derived vmDA progenitors (at DIV13—when approximately 50% of the culture is proliferating) were treated with ganciclovir (GCV) or saline for 5 days (Figure 5A). GCV-treated cultures had significantly less Ki67⁺ proliferative cells (−GCV: 18.34% ± 0.19% Ki67⁺ cells, +GCV: 7.84% ± 0.44%; Figure 5B). Importantly, activation of the suicide gene, by administration of the GCV, failed to evoke a response by the immune cells when H1-FS-8IM vmDA progenitors were co-cultured with PBMCs (Figures 5C and 5D). To test efficiency of the suicide gene system *in vivo*, nude mice received H1-FS-8IM neural grafts followed by daily administration of GCV (50 mg/kg i.p.) from week 8 to 9 post-transplant (Figure 5E). Human NCAM labeling revealed viable grafts after 9 weeks, with no difference in graft volume between the groups (Figures 5F and 5G). GCV-treated grafts showed a significant reduction in the proportion (2.14-fold) and the density (1.65-fold) of Ki67⁺ proliferative cells (−GCV: 22.52% ± 3.02% Ki67⁺/HNA⁺ cells, +GCV: 11.87% ± 2.77% Ki67⁺/HNA⁺ cells, $p = 0.0148$; Ki67 density: −GCV: 39,156 ± 3,255 cells/mm³, +GCV: 23,792 ± 7,033 cells/mm³, $p = 0.0471$; Figures 5H–5L). Within these immune-compromised host mice, no significant difference in the resident immune cell response was observed following GCV treatment (Figures 5M–5O), as previously reported.²⁶

Cloaked H1-FS-8IM-derived vmDA neurons are capable of reversing motor deficits and structurally integrating into the Parkinsonian rodent brain

Finally, we assess the capacity of H1-FS-8IM derived vmDA progenitors to structurally and functionally integrate into an immune-compromised athymic rat model of PD. The catecholamine-selective neurotoxin 6-hydroxydopamine (6-OHDA) was unilaterally injected into the vm to ablate the host dopamine system responsible for motor function. After 4 weeks, animals were assessed for amphetamine-induced motor asymmetry and only rats showing >6 rotations/min were included in the study. Rats were stratified into 3 groups: Lesion, Lesion + H1-FS vmDA progenitor graft (subsequently referred to as “H1-FS”) or Lesion + H1-FS-8IM vmDA progenitor graft (“H1-FS-8IM”), with behavioral testing at 16 and 20 weeks (Figure 6A).

At 16 weeks, both H1-FS- and H1-FS-8IM-derived neural grafts showed evidence of improved motor function, with complete reversal of rotational asymmetry by 20 weeks (Figure 6C). Post-mortem histochemical assessment at 20 weeks revealed viable grafts in all animals, with hNCAM-labeling highlighting the graft core predominantly confined to the host striatum and elaborate innervation throughout the dorsoventral and rostro-caudal axis of the striatum, the target tissue critical for reversal of motor deficits (Figure 6B). No significant difference in graft

size, total number of HNA⁺ cells, or cell density was observed (Figures 6D–6F). Similarly, neuronal counts (Figures 6G–6I), and more specifically TH⁺ DA neuron counts as well as the sub-populations of DA neurons within the grafts (A9-like TH⁺GIRK2⁺ and A10-like TH⁺CALB⁺) were not different between the two grafted groups (Figures 6K, 6L, and 6N). Employment of a human-specific TH antibody enabling distinction of the graft-derived DA fiber innervation, from residual host DA fibers, revealed comparable graft-derived host innervation (Figures 6J and 6M).

DISCUSSION

These results highlight the ability of cloaked human PSC-derived neurons to evade immune detection in a humanized mouse and reverse motor deficits in a Parkinsonian rat model, demonstrating the feasibility for a universal “off-the-shelf” cell product amenable to broad clinical application.

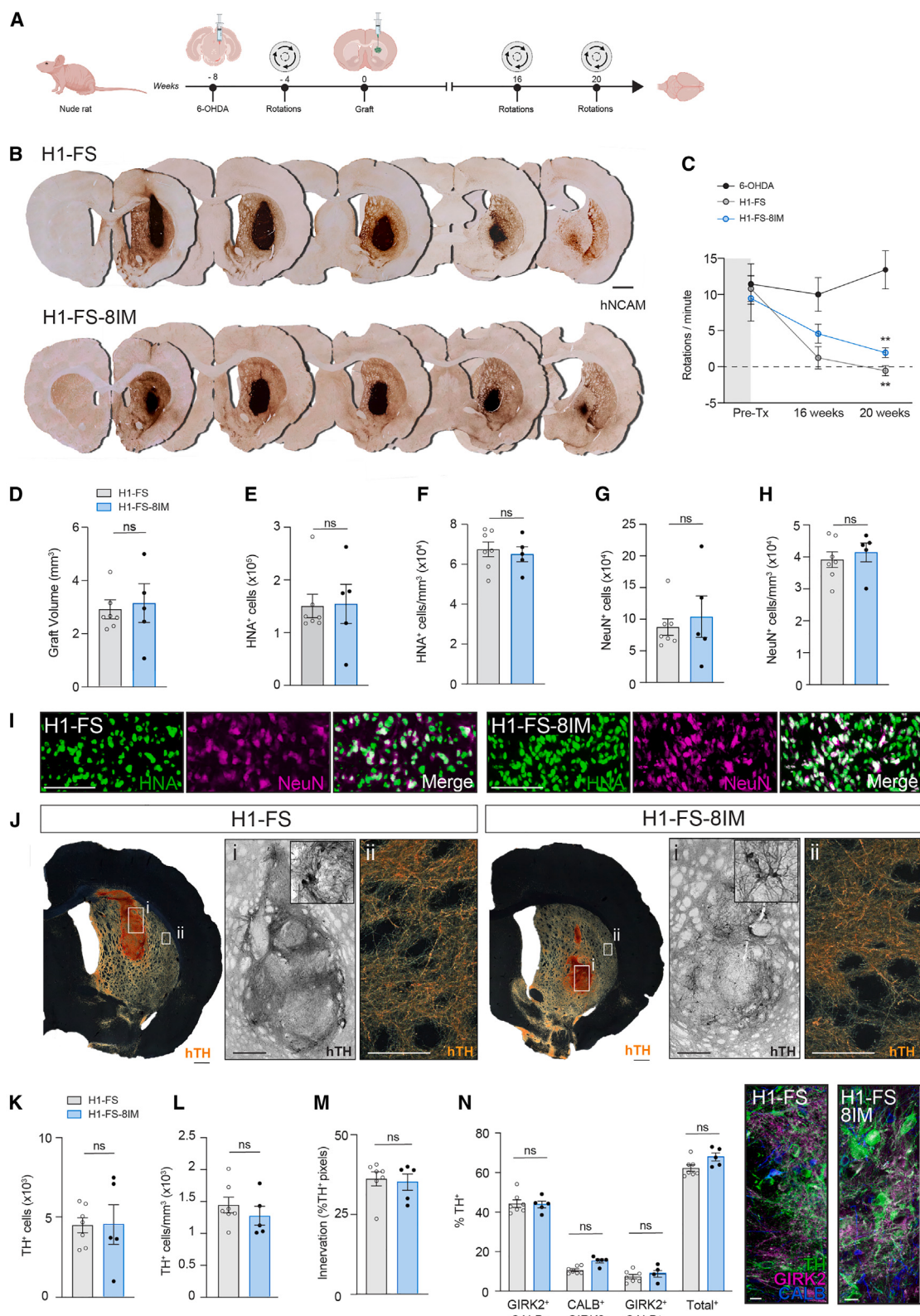
To date, assessment of the immunogenicity of dopamine progenitors, suitable for neural transplantation, has been variable and limited (see Qarin et al.³). Early studies reported initial undetectable expression of MHC class I and II molecules on human fetal vm tissue, yet upregulated expression upon pro-inflammatory cytokines exposure, as would be the environment at the graft site, rendering the cells susceptible to immune rejection.³⁹ Others have similarly reported immunological responses when fetal or PSC-derived neural progenitors (inclusive of vm-derived) were co-cultured with allogeneic PBMCs, causing T cell proliferation, but observed a minimal response when co-cultured with purified T cells,^{39–41} suggesting that neural progenitors are not capable of directly stimulating T cells, rather evoke a response through indirect allorecognition via host APCs. In contrast, others have reported that neural progenitors may be slightly immunosuppressive by secreting transforming growth factor β (TGF-β) that can inhibit T cell proliferation. Adopting a series of *in vitro* co-culture assays, here, we report the capability of human PSC-derived vmDA neural progenitors to evoke an immune response in the presence of multiple immune cell populations (T lymphocytes, NK cells, DCs, and macrophages), highlighting the necessity for immune modulation. Adopting the H1-FS-8IM hPSC line, we demonstrate that differentiated vmDA neural progenitors/neurons are capable of evading detection by all immune cell populations tested *in vitro*, as well as prevent elevated cytokine production.

Reflective of *in vitro* observations, transplantation of these cloaked H1-FS-8IM hPSC-derived neural progenitors into the HIS mouse showed similar prevention of immune cell proliferation and cytokine production (screened locally in the brain and peripherally within the CSF and blood plasma). The consequence was larger grafts containing more TH⁺ DA neurons and reduced resident reactive astrocytic and microglial density. The functionality of these cloaked vmDA neurons was confirmed

(M–O) Area of sampling for resident immune cell density. Density and representative images of (N) GFAP⁺ astroglia and (O) Iba1⁺ microglia at the graft-host interface showing no significant difference with or without GCV.

Data represent mean ± SEM, Mann-Whitney U test or Student's t test. (B) and (D) $n = 3$ independent cultures or (G)–(J) $n = 8$ grafts per group. Scale bars: (B), (K), (L), (N), and (O) 100 μm, (F) 1 mm, (K') and (L') 50 μm.

Abbreviations are as follows: DIV, days *in vitro*; CTV, cell trace violet; GCV, ganciclovir; HNA, human nuclear antigen; vmDA, ventral midbrain dopaminergic; PHA, phytohaemagglutinin.



(legend on next page)

by their ability to reverse motor deficits following engraftment into a rat unilateral model of dopamine depletion. In contrast, we report that the allogeneic transplantation of uncloaked human neural progenitors into a humanized mouse model evoked immune responses resulting in graft rejection. Such responses indicate that these allogeneic cells do express antigenic epitopes that can be trafficked to the periphery via glymphatic drainage and the meningeal lymphatic vessels to mount an immune response involving monocytes/macrophages, T and dendritic cells infiltration into the CNS, in addition to local attack by resident immune cells (microglia and astrocytes).

The present findings of an immune-evading donor cell suitable for neural transplantation are of significant relevance as the field awaits the outcome of a number of clinical trials that are adopting ≥ 1 immune-suppressant drug to combat graft rejection.^{42–44} The decision to adopt ≥ 12 months immune suppression stems from retrospective assessment of former clinical trials that employed a range of immune-suppressant regimens to preserve fetal tissue graft survival (see review Salado-Manzano et al.⁴⁵), with evidence that PD symptoms worsened in patients when cyclosporine administration was ceased 6 months after grafting.⁴⁶ Correspondingly, post-mortem analyses revealed activated microglia, astrogliosis, perivascular cuffing, B cells, T cells, and macrophages infiltration around the graft site.^{45–48} This current regimen however leaves a number of unknowns. Could antigens differ from fetal versus human PSC-derived neural donor cells? What are the implications for graft survival at more protracted time frames? And what considerations are there for the ongoing, underlying pathological state?

While previous studies have suggested allogeneic grafts of fetal vm tissue survival in the non-human primate brain without immune suppression,⁴⁹ more recent PSC-derived non-human primate allogeneic grafts have highlighted local microglia activation and leukocyte infiltration, leading to a low vmDA neurons survival, events that could be abrogated by administration of tacrolimus, a calcineurin inhibitor that suppresses T cells activation and cytokines production.^{50,51} Others have also argued that the initial inflammatory response to the surgical cell implantation is responsible for differential survival of DA neurons within hPSC-derived neural grafts, with evidence that co-trans-

plantation of autologous T regulatory cells could effectively reduce the needle-trauma-induced death of DA neurons—providing an additional means to improve clinical outcomes in the future.⁵²

The longevity of immune evasion and graft survival is also of critical importance as the progressive disease state is known to alter the immune state. This is of significant importance in the context of neurodegenerative diseases, with evidence that PD patients show changes in their peripheral immune system with ongoing disease advancement that could impact graft outcomes. PD patients present PBMCs producing more inflammatory cytokines, hyperactive monocytes and T regulatory cells with an impaired ability to suppress T cell function⁵³ that could manifest in enhanced T cell recruitment and graft rejection at protracted times. Such knowledge highlights the need for future studies to assess immune evasion in models that reflect the progressive pathological condition (unlike the acute dopamine depletion model of the disease adopted here); however, at present, this is confounded by the protracted nature of transgenic PD models (such as the human A53T model⁵⁴) and the need to generate a humanized immune state within these strains.

One needs also to consider possible drug-transplant interactions in patients. In xenografting studies, Levodopa (L-DOPA) administration (the primary treatment for motor symptoms) has been shown to elevate the immune response around the graft site, as well as that of circulating inflammatory cytokines including IL-1 β , IFN- γ , and TNF- α .⁵⁵ With the persistent use of L-DOPA in the majority of PD patients receiving grafts to date, the employment of cloaked grafts will circumvent such potential pharmacological-graft responses.

As immune modulation carries potential risks, namely tumors associated with “rogue” proliferative cells evading maturation and subsequent immune detection, here, we critically demonstrate the functionality of a FS suicide gene, additionally engineered into the universal donor cells, to ablate residual dividing cells within the graft. Adopting our previous approach,²⁶ the timely activation of the suicide switch (by early treatment with the prodrug ganciclovir) can also be exploited to enrich for early born dopamine neurons within the graft, while preventing the overgrowth of later born, non-dopamine cells, resulting in a graft

Figure 6. Cloaked H1-FS-8IM PSC-derived vmDA neural grafts are capable of structural and functional integration, reversing motor deficits in a Parkinsonian rat model

- (A) Schematic study design of 6-OHDA lesioning, neural transplantation, functional assessment, and histological analysis in athymic nude rats.
- (B) Representative images showing a H1-FS and H1-FS-8IM PSC-derived vmDA progenitor graft.
- (C) Unilateral 6-OHDA-lesioned rats showed sustained rotational asymmetry upon amphetamine challenge (black line), that could be reversed by 20 weeks post-transplantation in animals receiving H1-FS (gray) or H1-FS-8IM (blue) PSC-derived vmDA progenitor grafts.
- (D–H) (D) Quantification of graft volume, (E) total HNA $^+$ cells, (F) density of HNA $^+$ cells, (G) total NeuN $^+$ neurons, and (H) neuronal density revealed comparable graft size and composition at 8 weeks in immunodeficient rats grafted receiving uncloaked (gray) or cloaked (blue) neural grafts.
- (I) Representative images showing comparable density of cells (HNA $^+$) and neurons (NeuN $^+$) within grafts.
- (J) Dark field images showing hTH staining from a representative H1-FS and (K) H1-FS-8IM PSC-derived neural graft. Inserts (I) show TH $^+$ cell density and (ii) density of TH $^+$ fibers within the dorsolateral striatum.
- (K–M) (K) Reflective of comparable functional recovery, TH $^+$ DA neuron numbers, (L) their density, and (M) the density of human TH $^+$ fiber innervation in the dorsolateral striatum remained unchanged between animals grafted with uncloaked or cloaked vmDA progenitors.
- (N) The proportion of TH $^+$ cells maturing into GIRK2-expressing and/or Calbindin-expressing DA neurons was comparable within H1-FS- and H1-FS-8IM hPSC-derived vmDA progenitor grafts.

Data represent mean \pm SEM, Mann-Whitney U test or Student's t test. (B)–(N) $n = 5$ –7 grafted animals/group. ** $p < 0.01$. Scale bars: (B) and (J) 1 mm; (I) 50 μ m; (J)–(iii) 100 μ m; (N) 100 μ m.

Abbreviations are as follows: 6-OHDA, 6-hydroxydopamine; CALB, Calbindin; hNCAM, human neural cell adhesion molecule; HNA, human nuclear antigen; NeuN, neuronal nuclei; pre-Tx, pre-transplantation; hTH, human-specific tyrosine hydroxylase.

of more predictable composition, greater purity, and consequently anticipated functionality.

We acknowledge that a number of approaches have been adopted to generate immune-evasive donor cells by genome editing and wish to highlight that the approach presented here is to be considered complementing and not competing, recognizing that each approach presents its own advantages and limitations—see Hotta et al.¹⁸ Overall, the ability to employ a single universal PSCs, such as the H1-FS-8IM line, will ultimately expand the candidate pool of patients for neural grafting, not only in the treatment of PD but for a plethora of other neurological conditions for which cell-based therapies are a feasible consideration, such as stroke, epilepsy, and Huntington's disease.

Limitations of the study

In current and planned clinical trials, the long-term survival of grafts and the impact of host immune response beyond the periods of immune suppression in PD patients remain unknown. Unfortunately, limitations in the humanized mouse model adopted in this study prevented assessment of the grafts at more protracted periods, as these animals possessed only partial reconstitution via human CD34⁺ hematopoietic stem/progenitor cells (HSPCs), with the proportion of circulating human immune cells diminishing with time⁵⁶ (Figure S6B). In recent years, a number of new and improved humanized mouse models have been established that will enable greater interrogation of immunological responses,⁵⁷ yet each comes with benefits and limitations and selection will therefore depend on the questions at hand—for further insight into these models see Martinov et al.⁵⁸ For these reasons, it will therefore be important to, in parallel, assess allogeneic grafts using non-human primate PSC-derived neural progenitors engineered for comparable cloaking to the H1-FS-8IM line described here, noting the increase in marmoset PSC lines in recent years that renders this a plausible option, and the successful efforts to generate vmDA neurons.⁵⁹

RESOURCE AVAILABILITY

Lead contact

Requests for further information and resources should be directed to and will be fulfilled by the lead contact, Clare Parish (cparish@unimelb.edu.au).

Materials availability

The H1-FS-8IM and H1-FS human pluripotent stem cell line will be made available upon request to co-author Andras Nagy (NAGY@lunenfeld.ca).

Data and code availability

The authors declare that the data supporting the findings of this study are presented within the paper and its supplemental information files. Source data will be shared upon request. No code was generated in this study.

ACKNOWLEDGMENTS

The authors thank Mong Tien and Brianna Xuereb (the Florey Institute for Neuroscience and Mental Health, Australia, FINMH) for expert technical assistance, Dr. Eric Jong for removing fluorescent selectable markers from the original H1-FS-8IM cell line, Merle Dayton for assistance in generating the HIS mice, and Dr. Ben Gu for supplying the blood samples. We acknowledge the support of the flow cytometry facility at the Melbourne Brain Centre, Australia and the Florey Microscopy Facility. C.L.P. was supported by a National Health and Medical Research Council Australia (NHMRC) Senior Research

Fellowship and NHMRC Level 2 Fellowship. This work was supported by grant funding from the NHMRC (GNT2026395). The FINMH acknowledges the strong support from the Victorian Government and funding from the Operational Infrastructure Support Grant. A.N. was supported by Medicine by Design (University of Toronto), funding by the Ontario Research Fund (MRI ORF RE08-064 SEPT2021) and by seed fund from Monash University. Development of myeloid models was supported by a NHMRC synergy grant (APP1186371) to C.A.W.

AUTHOR CONTRIBUTIONS

C.P. and C.L.P. conceived the experiments and wrote the manuscript; C.P., K.C.D., N.P., S.F., C.P.J.H., N.M., K.D.A.-B., M.Á.B.R., Z.E., L.W., W.C., H.Y., and C.L.P. performed experiments; M.P., C.A.W., L.H.T., A.N., and C.L.P. provided reagents and expertise; all authors reviewed/edited the manuscript; C.L.P. provided funding.

DECLARATION OF INTERESTS

A.N. is an inventor on the patent application covering the induced Allogeneic Cell Tolerance (IACT Stealth) Technology (WO/2018/227286) and the patent covering the safe-cell (FailSafe) technology (PCT/CA2016/050256). A.N. is a co-founder and shareholder of panCELLa Inc, having exclusive license to the technology.

STAR METHODS

Detailed methods are provided in the online version of this paper and include the following:

- [KEY RESOURCES TABLE](#)
- [EXPERIMENTAL MODEL AND STUDY PARTICIPANT DETAILS](#)
 - Rodents
 - Human embryonic stem cells
 - Immune cells
- [METHOD DETAILS](#)
 - Generation, validation and culture of H1-FS-8IM PSCs
 - Generation and co-culture of immune cell populations
 - Surgical Procedures
 - Behavioural Testing
 - Tissue isolation
 - Immunophenotyping
 - Tissue Processing and Immunohistochemistry
- [QUANTIFICATION AND STATISTICAL ANALYSIS](#)

SUPPLEMENTAL INFORMATION

Supplemental information can be found online at <https://doi.org/10.1016/j.stem.2025.03.008>.

Received: April 5, 2024

Revised: November 13, 2024

Accepted: March 13, 2025

Published: April 9, 2025

REFERENCES

1. Steinbeck, J.A., and Studer, L. (2015). Moving stem cells to the clinic: potential and limitations for brain repair. *Neuron* 86, 187–206. <https://doi.org/10.1016/j.neuron.2015.03.002>.
2. Barker, R.A., Parmar, M., Studer, L., and Takahashi, J. (2017). Human Trials of Stem Cell-Derived Dopamine Neurons for Parkinson's Disease: Dawn of a New Era. *Cell Stem Cell* 21, 569–573. <https://doi.org/10.1016/j.stem.2017.09.014>.
3. Qarin, S., Howlett, S.K., Jones, J.L., and Barker, R.A. (2021). The immunogenicity of midbrain dopaminergic neurons and the implications for neural

- grafting trials in Parkinson's disease. *Neuronal Signal.* 5, NS20200083. <https://doi.org/10.1042/NS20200083>.
4. Sloan, D.J., Wood, M.J., and Charlton, H.M. (1991). The immune response to intracerebral neural grafts. *Trends Neurosci.* 14, 341–346. [https://doi.org/10.1016/0166-2236\(91\)90159-r](https://doi.org/10.1016/0166-2236(91)90159-r).
 5. Louveau, A., Harris, T.H., and Kipnis, J. (2015). Revisiting the Mechanisms of CNS Immune Privilege. *Trends Immunol.* 36, 569–577. <https://doi.org/10.1016/j.it.2015.08.006>.
 6. Riminton, D.S., Hartung, H.P., and Reddel, S.W. (2011). Managing the risks of immunosuppression. *Curr. Opin. Neurol.* 24, 217–223. <https://doi.org/10.1097/WCO.0b013e328346d47d>.
 7. Lanza, R., Russell, D.W., and Nagy, A. (2019). Engineering universal cells that evade immune detection. *Nat. Rev. Immunol.* 19, 723–733. <https://doi.org/10.1038/s41577-019-0200-1>.
 8. Taylor, C.J., Peacock, S., Chaudhry, A.N., Bradley, J.A., and Bolton, E.M. (2012). Generating an iPSC bank for HLA-matched tissue transplantation based on known donor and recipient HLA types. *Cell Stem Cell* 11, 147–152. <https://doi.org/10.1016/j.stem.2012.07.014>.
 9. Nakatsui, N., Nakajima, F., and Tokunaga, K. (2008). HLA-haplotype banking and iPS cells. *Nat. Biotechnol.* 26, 739–740. <https://doi.org/10.1038/nbt0708-739>.
 10. Morizane, A., Kikuchi, T., Hayashi, T., Mizuma, H., Takara, S., Doi, H., Mawatari, A., Glasser, M.F., Shiina, T., Ishigaki, H., et al. (2017). MHC matching improves engraftment of iPSC-derived neurons in non-human primates. *Nat. Commun.* 8, 385. <https://doi.org/10.1038/s41467-017-00926-5>.
 11. Xu, H., Wang, B., Ono, M., Kagita, A., Fujii, K., Sasakawa, N., Ueda, T., Gee, P., Nishikawa, M., Nomura, M., et al. (2019). Targeted Disruption of HLA Genes via CRISPR-Cas9 Generates iPSCs with Enhanced Immune Compatibility. *Cell Stem Cell* 24, 566–578.e7. <https://doi.org/10.1016/j.stem.2019.02.005>.
 12. Gornalusse, G.G., Hirata, R.K., Funk, S.E., Riobolos, L., Lopes, V.S., Manske, G., Prunkard, D., Colunga, A.G., Hanafi, L.A., Clegg, D.O., et al. (2017). HLA-E-expressing pluripotent stem cells escape allogeneic responses and lysis by NK cells. *Nat. Biotechnol.* 35, 765–772. <https://doi.org/10.1038/nbt.3860>.
 13. Deuse, T., Hu, X., Gravina, A., Wang, D., Tedashvili, G., De, C., Thayer, W.O., Wahl, A., Garcia, J.V., Reichenspurner, H., et al. (2019). Hypoimmunogenic derivatives of induced pluripotent stem cells evade immune rejection in fully immunocompetent allogeneic recipients. *Nat. Biotechnol.* 37, 252–258. <https://doi.org/10.1038/s41587-019-0016-3>.
 14. Han, X., Wang, M., Duan, S., Franco, P.J., Kenty, J.H.R., Hedrick, P., Xia, Y., Allen, A., Ferreira, L.M.R., Strominger, J.L., et al. (2019). Generation of hypoimmunogenic human pluripotent stem cells. *Proc. Natl. Acad. Sci. USA* 116, 10441–10446. <https://doi.org/10.1073/pnas.1902566116>.
 15. Bashor, C.J., Hilton, I.B., Bandukwala, H., Smith, D.M., and Veiseh, O. (2022). Engineering the next generation of cell-based therapeutics. *Nat. Rev. Drug Discov.* 21, 655–675. <https://doi.org/10.1038/s41573-022-00476-6>.
 16. Zhang, Q., and Reed, E.F. (2016). The importance of non-HLA antibodies in transplantation. *Nat. Rev. Nephrol.* 12, 484–495. <https://doi.org/10.1038/nrneph.2016.88>.
 17. Hu, X., Gattis, C., Olroyd, A.G., Friera, A.M., White, K., Young, C., Basco, R., Lamba, M., Wells, F., Ankala, R., et al. (2023). Human hypoimmune primary pancreatic islets avoid rejection and autoimmunity and alleviate diabetes in allogeneic humanized mice. *Sci. Transl. Med.* 15, eadg5794. <https://doi.org/10.1126/scitranslmed.adg5794>.
 18. Hotta, A., Schrepfer, S., and Nagy, A. (2024). Genetically engineered hypoimmunogenic cell therapy. *Nat. Rev. Bioeng.* 2, 960–979. <https://doi.org/10.1038/s44222-024-00219-9>.
 19. King, A., Burrows, T.D., Hiby, S.E., Bowen, J.M., Joseph, S., Verma, S., Lim, P.B., Gardner, L., Le Bouteiller, P., Ziegler, A., et al. (2000). Surface expression of HLA-C antigen by human extravillous trophoblast. *Placenta* 21, 376–387. <https://doi.org/10.1053/plac.1999.0496>.
 20. Ander, S.E., Diamond, M.S., and Coyne, C.B. (2019). Immune responses at the maternal-fetal interface. *Sci. Immunol.* 4, eaat6114. <https://doi.org/10.1126/sciimmunol.aat6114>.
 21. Wiedemann, M., and Voehringer, D. (2020). Immunomodulation and Immune Escape Strategies of Gastrointestinal Helminths and Schistosomes. *Front. Immunol.* 11, 572865. <https://doi.org/10.3389/fimmu.2020.572865>.
 22. Ernst, J.D. (2018). Mechanisms of *M. tuberculosis* Immune Evasion as Challenges to TB Vaccine Design. *Cell Host Microbe* 24, 34–42. <https://doi.org/10.1016/j.chom.2018.06.004>.
 23. Stammnitz, M.R., Coorens, T.H.H., Gori, K.C., Hayes, D., Fu, B., Wang, J., Martin-Herranz, D.E., Alexandrov, L.B., Baez-Ortega, A., Barthorpe, S., et al. (2018). The Origins and Vulnerabilities of Two Transmissible Cancers in Tasmanian Devils. *Cancer Cell* 33, 607–619.e15. <https://doi.org/10.1016/j.ccr.2018.03.013>.
 24. Harding, J., Vintersten-Nagy, K., Yang, H., Tang, J.K., Shutova, M., Jong, E.D., Lee, J.H., Massumi, M., Oussenko, T., Izadifar, Z., et al. (2024). Immune-privileged tissues formed from immunologically cloaked mouse embryonic stem cells survive long term in allogeneic hosts. *Nat. Biomed. Eng.* 8, 427–442. <https://doi.org/10.1038/s41551-023-01133-y>.
 25. Liang, Q., Monetti, C., Shutova, M.V., Neely, E.J., Hacibekiroglu, S., Yang, H., Kim, C., Zhang, P., Li, C., Nagy, K., et al. (2018). Linking a cell-division gene and a suicide gene to define and improve cell therapy safety. *Nature* 563, 701–704. <https://doi.org/10.1038/s41586-018-0733-7>.
 26. de Luzy, I.R., Law, K.C.L., Moriarty, N., Hunt, C.P.J., Durnall, J.C., Thompson, L.H., Nagy, A., and Parish, C.L. (2021). Human stem cells harboring a suicide gene improve the safety and standardisation of neural transplants in Parkinsonian rats. *Nat. Commun.* 12, 3275. <https://doi.org/10.1038/s41467-021-23125-9>.
 27. Spivey, T.L., Uccellini, L., Ascierto, M.L., Zoppoli, G., De Giorgi, V., Delogu, L.G., Engle, A.M., Thomas, J.M., Wang, E., Marincola, F.M., et al. (2011). Gene expression profiling in acute allograft rejection: challenging the immunologic constant of rejection hypothesis. *J. Transl. Med.* 9, 174. <https://doi.org/10.1186/1479-5876-9-174>.
 28. Alves de Lima, K., Rustenhoven, J., and Kipnis, J. (2020). Meningeal Immunity and Its Function in Maintenance of the Central Nervous System in Health and Disease. *Annu. Rev. Immunol.* 38, 597–620. <https://doi.org/10.1146/annurev-immunol-102319-103410>.
 29. Sun, J., Bird, C.H., Sutton, V., McDonald, L., Coughlin, P.B., De Jong, T.A., Trapani, J.A., and Bird, P.I. (1996). A cytosolic granzyme B inhibitor related to the viral apoptotic regulator cytokine response modifier A is present in cytotoxic lymphocytes. *J. Biol. Chem.* 271, 27802–27809. <https://doi.org/10.1074/jbc.271.44.27802>.
 30. Matozaki, T., Murata, Y., Okazawa, H., and Ohnishi, H. (2009). Functions and molecular mechanisms of the CD47-SIRPalpha signalling pathway. *Trends Cell Biol.* 19, 72–80. <https://doi.org/10.1016/j.tcb.2008.12.001>.
 31. Nathan, C., and Muller, W.A. (2001). Putting the brakes on innate immunity: a regulatory role for CD200? *Nat. Immunol.* 2, 17–19. <https://doi.org/10.1038/383124>.
 32. Calvanese, V., Capellera-Garcia, S., Ma, F., Fares, I., Liebscher, S., Ng, E.S., Ekstrand, S., Aguadé-Gorgorió, J., Vavilina, A., Lefauveaux, D., et al. (2022). Mapping human hematopoietic stem cells from haemogenic endothelium to birth. *Nature* 604, 534–540. <https://doi.org/10.1038/s41586-022-04571-x>.
 33. Rajab, N., Angel, P.W., Deng, Y., Gu, J., Jameson, V., Kurowska-Stolarska, M., Milling, S., Pacheco, C.M., Rutar, M., Laslett, A.L., et al. (2021). An integrated analysis of human myeloid cells identifies gaps in *in vitro* models of *in vivo* biology. *Stem Cell Rep.* 16, 1629–1643. <https://doi.org/10.1016/j.stemcr.2021.04.010>.
 34. Mangan, M.S., Melo-Silva, C.R., Luu, J., Bird, C.H., Koskinen, A., Rizzitelli, A., Prakash, M., Scarff, K.L., Müllbacher, A., Regner, M., et al. (2017). A pro-survival role for the intracellular granzyme B inhibitor Serpinb9 in natural killer cells during poxvirus infection. *Immunol. Cell Biol.* 95, 884–894. <https://doi.org/10.1038/icb.2017.59>.

35. Smyth, M.J., Sullivan, L.C., Brooks, A.G., and Andrews, D.M. (2013). Non-classical MHC Class I molecules regulating natural killer cell function. *Oncol Immunol* 2, e23336. <https://doi.org/10.4161/onci.23336>.
36. Benichou, G., Yamada, Y., Aoyama, A., and Madsen, J.C. (2011). Natural killer cells in rejection and tolerance of solid organ allografts. *Curr Opin Organ Transplant* 16, 47–53. <https://doi.org/10.1097/MOT.0b013e32834254cf>.
37. Förster, R., Davalos-Misslitz, A.C., and Rot, A. (2008). CCR7 and its ligands: balancing immunity and tolerance. *Nat Rev Immunol* 8, 362–371. <https://doi.org/10.1038/nri2297>.
38. Shields, J.D., Kourtis, I.C., Tomei, A.A., Roberts, J.M., and Swartz, M.A. (2010). Induction of lymphoidlike stroma and immune escape by tumors that express the chemokine CCL21. *Science* 328, 749–752. <https://doi.org/10.1126/science.1185837>.
39. Laguna Goya, R., Busch, R., Mathur, R., Coles, A.J., and Barker, R.A. (2011). Human fetal neural precursor cells can up-regulate MHC class I and class II expression and elicit CD4 and CD8 T cell proliferation. *Neurobiol Dis* 47, 407–414. <https://doi.org/10.1016/j.nbd.2010.10.008>.
40. Ozaki, M., Iwanami, A., Nagoshi, N., Kohyama, J., Itakura, G., Iwai, H., Nishimura, S., Nishiyama, Y., Kawabata, S., Sugai, K., et al. (2017). Evaluation of the immunogenicity of human iPS cell-derived neural stem/progenitor cells in vitro. *Stem Cell Res* 19, 128–138. <https://doi.org/10.1016/j.scr.2017.01.007>.
41. Liu, J., Götherström, C., Forsberg, M., Samuelsson, E.B., Wu, J., Calzarossa, C., Hovatta, O., Sundström, E., and Åkesson, E. (2013). Human neural stem/progenitor cells derived from embryonic stem cells and fetal nervous system present differences in immunogenicity and immunomodulatory potentials in vitro. *Stem Cell Res* 10, 325–337. <https://doi.org/10.1016/j.scr.2013.01.001>.
42. Piao, J., Zabierowski, S., Dubose, B.N., Hill, E.J., Navare, M., Claros, N., Rosen, S., Ramnarine, K., Horn, C., Fredrickson, C., et al. (2021). Preclinical Efficacy and Safety of a Human Embryonic Stem Cell-Derived Midbrain Dopamine Progenitor Product, MSK-DA01. *Cell Stem Cell* 28, 217–229.e7. <https://doi.org/10.1016/j.stem.2021.01.004>.
43. Takahashi, J. (2020). iPS cell-based therapy for Parkinson's disease: A Kyoto trial. *Regen Ther* 13, 18–22. <https://doi.org/10.1016/j.reth.2020.06.002>.
44. Kirkeby, A., Nelander, J., Hoban, D.B., Rogelius, N., Bjartmarz, H., Novo Nordisk Cell Therapy R&D, Storm, P., Fiorenzano, A., Adler, A.F., and Vale, S. (2023). Preclinical quality, safety, and efficacy of a human embryonic stem cell-derived product for the treatment of Parkinson's disease, STEM-PD. *Cell Stem Cell* 30, 1299–1314.e9. <https://doi.org/10.1016/j.stem.2023.08.014>.
45. Salado-Manzano, C., Perpiña, U., Straccia, M., Molina-Ruiz, F.J., Cozzi, E., Rosser, A.E., and Canals, J.M. (2020). Is the Immunological Response a Bottleneck for Cell Therapy in Neurodegenerative Diseases? *Front Cell Neurosci* 14, 250. <https://doi.org/10.3389/fncel.2020.00250>.
46. Olanow, C.W., Goetz, C.G., Kordower, J.H., Stoessl, A.J., Sossi, V., Brin, M.F., Shannon, K.M., Nauert, G.M., Perl, D.P., Godbold, J., et al. (2003). A double-blind controlled trial of bilateral fetal nigral transplantation in Parkinson's disease. *Ann Neurol* 54, 403–414. <https://doi.org/10.1002/ana.10720>.
47. Freed, C.R., Greene, P.E., Breeze, R.E., Tsai, W.Y., DuMouchel, W., Kao, R., Dillon, S., Winfield, H., Culver, S., Trojanowski, J.Q., et al. (2001). Transplantation of embryonic dopamine neurons for severe Parkinson's disease. *N Engl J Med* 344, 710–719. <https://doi.org/10.1056/NEJM200103083441002>.
48. Kordower, J.H., Freeman, T.B., Snow, B.J., Vingerhoets, F.J., Mufson, E.J., Sanberg, P.R., Hauser, R.A., Smith, D.A., Nauert, G.M., and Perl, D.P. (1995). Neuropathological evidence of graft survival and striatal reinnervation after the transplantation of fetal mesencephalic tissue in a patient with Parkinson's disease. *N Engl J Med* 332, 1118–1124. <https://doi.org/10.1056/NEJM199504273321702>.
49. Redmond, D.E., Jr., Vinuela, A., Kordower, J.H., and Isaacson, O. (2008). Influence of cell preparation and target location on the behavioral recovery after striatal transplantation of fetal dopaminergic neurons in a primate model of Parkinson's disease. *Neurobiol Dis* 29, 103–116. <https://doi.org/10.1016/j.nbd.2007.08.008>.
50. Morizane, A., Doi, D., Kikuchi, T., Okita, K., Hotta, A., Kawasaki, T., Hayashi, T., Onoe, H., Shiina, T., Yamanaka, S., et al. (2013). Direct comparison of autologous and allogeneic transplantation of iPSC-derived neural cells in the brain of a non-human primate. *Stem Cell Rep* 1, 283–292. <https://doi.org/10.1016/j.stemcr.2013.08.007>.
51. Kikuchi, T., Morizane, A., Doi, D., Magotani, H., Onoe, H., Hayashi, T., Mizuma, H., Takara, S., Takahashi, R., Inoue, H., et al. (2017). Human iPS cell-derived dopaminergic neurons function in a primate Parkinson's disease model. *Nature* 548, 592–596. <https://doi.org/10.1038/nature23664>.
52. Park, T.Y., Jeon, J., Lee, N., Kim, J., Song, B., Kim, J.H., Lee, S.K., Liu, D., Cha, Y., Kim, M., et al. (2023). Co-transplantation of autologous Treg cells in a cell therapy for Parkinson's disease. *Nature* 619, 606–615. <https://doi.org/10.1038/s41586-023-06300-4>.
53. Tansey, M.G., Wallings, R.L., Houser, M.C., Herrick, M.K., Keating, C.E., and Joers, V. (2022). Inflammation and immune dysfunction in Parkinson disease. *Nat Rev Immunol* 22, 657–673. <https://doi.org/10.1038/s41577-022-00684-6>.
54. Cenci, M.A., and Björklund, A. (2020). Animal models for preclinical Parkinson's research: an update and critical appraisal. *Prog Brain Res* 252, 27–59. <https://doi.org/10.1016/bs.pbr.2020.02.003>.
55. Breger, L.S., Kienle, K., Smith, G.A., Dunnett, S.B., and Lane, E.L. (2017). Influence of chronic L-DOPA treatment on immune response following allogeneic and xenogeneic graft in a rat model of Parkinson's disease. *Brain Behav Immun* 61, 155–164. <https://doi.org/10.1016/j.bbi.2016.11.014>.
56. Hess, N.J., Brown, M.E., and Capitini, C.M. (2021). GVHD Pathogenesis, Prevention and Treatment: Lessons From Humanized Mouse Transplant Models. *Front Immunol* 12, 723544. <https://doi.org/10.3389/fimmu.2021.723544>.
57. Kooreman, N.G., de Almeida, P.E., Stack, J.P., Nelakanti, R.V., Diecke, S., Shao, N.Y., Swijnenburg, R.J., Sanchez-Freire, V., Matsa, E., Liu, C., et al. (2017). Alloimmune Responses of Humanized Mice to Human Pluripotent Stem Cell Therapeutics. *Cell Rep* 20, 1978–1990. <https://doi.org/10.1016/j.celrep.2017.08.003>.
58. Martinov, T., McKenna, K.M., Tan, W.H., Collins, E.J., Kehret, A.R., Linton, J.D., Olsen, T.M., Shobaki, N., and Rongvaux, A. (2021). Building the Next Generation of Humanized Hemato-Lymphoid System Mice. *Front Immunol* 12, 643852. <https://doi.org/10.3389/fimmu.2021.643852>.
59. Vermilyea, S.C., Guthrie, S., Meyer, M., Smuga-Otto, K., Braun, K., Howden, S., Thomson, J.A., Zhang, S.C., Emborg, M.E., and Golos, T.G. (2017). Induced Pluripotent Stem Cell-Derived Dopaminergic Neurons from Adult Common Marmoset Fibroblasts. *Stem Cells Dev* 26, 1225–1235. <https://doi.org/10.1089/scd.2017.0069>.
60. Watmuff, B., Hartley, B.J., Hunt, C.P.J., Fabb, S.A., Pouton, C.W., and Haynes, J.M. (2015). Human pluripotent stem cell derived midbrain PITX3(eGFP/w) neurons: a versatile tool for pharmacological screening and neurodegenerative modeling. *Front Cell Neurosci* 9, 104. <https://doi.org/10.3389/fncel.2015.00104>.
61. Arandjelovic, P., Kim, Y., Cooney, J.P., Preston, S.P., Doerflinger, M., McMahon, J.H., Garner, S.E., Zerbato, J.M., Roche, M., Tumpach, C., et al. (2023). Venetoclax, alone and in combination with the BH3 mimetic S63845, depletes HIV-1 latently infected cells and delays rebound in humanized mice. *Cell Rep Med* 4, 101178. <https://doi.org/10.1016/j.xcrm.2023.101178>.
62. Ganther, C.W., Cota-Coronado, A., Thompson, L.H., and Parish, C.L. (2020). An Optimized Protocol for the Generation of Midbrain Dopamine Neurons under Defined Conditions. *Star Protoc* 1, 100065. <https://doi.org/10.1016/j.xpro.2020.100065>.
63. Berrocal-Rubio, M.A., Pawer, Y.D.J., Dinevska, M., De Paoli-Iseppi, R., Widodo, S.S., Gleeson, J., Rajab, N., De Nardo, W., Hallab, J., Li, A., Mantamadiotis, T., Clark, M.B., and Wells, C.A. (2024). Discovery of

- NRG1-VII: a novel myeloid-derived class of NRG1. *BMC Genomics* 25, 814. <https://doi.org/10.1186/s12864-024-10723-2>.
64. Niclis, J.C., Gantner, C.W., Alsanie, W.F., McDougall, S.J., Bye, C.R., Elefanti, A.G., Stanley, E.G., Haynes, J.M., Pouton, C.W., Thompson, L.H., et al. (2017). Efficiently Specified Ventral Midbrain Dopamine Neurons from Human Pluripotent Stem Cells Under Xeno-Free Conditions Restore Motor Deficits in Parkinsonian Rodents. *Stem Cells Transl. Med.* 6, 937–948. <https://doi.org/10.5966/sctm.2016-0073>.
65. Elahi, Z., Jameson, V., Sakkas, M., Butcher, S.K., Mintern, J.D., Radford, K.J., and Wells, C.A. (2024). Efficient generation of human dendritic cells from iPSC by introducing a feeder-free expansion step for hematopoietic progenitors. Preprint at bioRxiv. <https://doi.org/10.1101/2024.06.04.594010>.
66. Gantner, C.W., de Luzy, I.R., Kauhausen, J.A., Moriarty, N., Niclis, J.C., Bye, C.R., Penna, V., Hunt, C.P.J., Ermine, C.M., Pouton, C.W., et al. (2020). Viral Delivery of GDNF Promotes Functional Integration of Human Stem Cell Grafts in Parkinson's Disease. *Cell Stem Cell* 26, 511–526.e5. <https://doi.org/10.1016/j.stem.2020.01.010>.

STAR★METHODS

KEY RESOURCES TABLE

REAGENT or RESOURCE	SOURCE	IDENTIFIER
Antibodies		
Mouse monoclonal anti-Calbindin-C28K (1:1000)	Swant	Cat# 300; RRID: AB_10000347
Rabbit monoclonal anti-Cleaved Caspase-3 (1:1000)	Cell Signaling	Cat# 9664; RRID: AB_2070042
Mouse monoclonal anti-CD1c, PE/Dazzle(TM) 594 conjugated (1:200)	Biolegend	Cat# 331532; RRID: AB_2565293
Mouse monoclonal anti-CD11c, PE/Cyanine7 conjugated (1:200)	Biolegend	Cat# 337216; RRID: AB_2129790
Mouse monoclonal anti-CD14, Pacific Blue conjugated (1:100)	BD Biosciences	Cat# 558121; RRID: AB_397041
Mouse monoclonal anti-CD19, BV510 conjugated (1:50)	BD Biosciences	Cat# 562947; RRID: AB_2737912
Mouse monoclonal anti-CD3, PE-Cy7 conjugated (1:100)	BD Biosciences	Cat# 557851; RRID: AB_396896
Mouse monoclonal anti-CD3, APC conjugated (1:100)	Biolegend	Cat# 300311; RRID: AB_314047
Mouse monoclonal anti-CD4, APC-H7 conjugated (1:100)	BD Biosciences	Cat# 560158; RRID: AB_1645478
Mouse monoclonal anti-CD4, PE-conjugated (1:100)	Biolegend	Cat# 344605; RRID: AB_1937247
Mouse monoclonal anti-CD45 (1:1000)	Thermo Fisher Scientific	Cat# 14-0451-82; RRID: AB_467251
Mouse monoclonal anti-CD45, BV786 conjugated (1:100)	BD Biosciences	Cat# 563716; RRID: AB_2716864
Mouse monoclonal anti-CD45, FITC-conjugated (1:100)	Biolegend	Cat# 304005; RRID: AB_314393
Mouse monoclonal anti-CD45.1, PE-conjugated (1:100)	BD Biosciences	Cat# 553776; RRID: AB_395044
Mouse monoclonal anti-CD45RO, PE-CF594 conjugated (1:100)	BD Biosciences	Cat# 562299; RRID: AB_1115439
Mouse monoclonal anti-CD56, PE-Cy7 conjugated (1:200)	Biolegend	Cat# 362509; RRID: AB_2563926
Mouse monoclonal anti-CD62L, PE-Cy5 conjugated (1:100)	BD Biosciences	Cat# 555545; RRID: AB_395929
Mouse monoclonal anti-CD8, APC conjugated (1:50)	BD Biosciences	Cat# 555369; RRID: AB_398595
Goat polyclonal anti-E-Cadherin (1:1000)	R&D Systems	Cat# AF748; RRID: AB_355568
Goat polyclonal anti-Foxa2 (1:200)	Santa Cruz Biotechnology	Cat# sc-6554; RRID: AB_2262810
Chicken polyclonal anti-GFAP (1:1000)	Thermo Fisher Scientific	Cat# # PA1-10004; RRID: AB_1074620
Goat polyclonal anti-GIRK2 (1:500)	Abcam	Cat# ab65096; RRID: AB_1139732
Mouse monoclonal anti-Human nuclear antigen (1:300)	Millipore	Cat# MAB1281; RRID: AB_94090
Rabbit monoclonal anti-Human nuclear antigen (1:1000)	NeoBiotechnologies	Cat# RBM5-346; RRID: AB_3662705
Rabbit polyclonal anti-Iba1 (1:1000)	FUJIFILM Wako Pure Chemical Corporation	Cat# 019-19741; RRID: AB_839504
Rat monoclonal anti-Ki-67 (1:1000)	Thermo Fisher Scientific	Cat# 14-5698-80; RRID: AB_10853185
Mouse monoclonal anti-LMX1A (1:1000)	Kind gift from Novo Nordisk	N/A
Chicken polyclonal anti-MAP2 (1:1000)	Thermo Fisher Scientific	Cat# PA1-10005; RRID: AB_1076848
Rabbit polyclonal anti-NANOG (1:200)	Proteintech	Cat# 14295-1-AP; RRID: AB_1607719
Mouse monoclonal anti-Nestin (1:1000)	Millipore	Cat# MAB353; RRID: AB_94911
Rabbit monoclonal anti-NeuN (1:1000)	Abcam	Cat# ab236869
Chicken polyclonal anti-NeuN (1:1000)	Millipore	Cat# ABN91; RRID: AB_11205760
Mouse monoclonal anti-Oct3/4 (1:100)	Santa Cruz Biotechnology	Cat# sc-5279; RRID: AB_628051
Goat polyclonal anti-Otx2 (1:500)	R&D Systems	Cat# AF1979; RRID: AB_2157172
Mouse monoclonal anti-PSA Ncam (Eric1) (1:500)	Santa Cruz Biotechnology	Cat# sc-106; RRID: AB_627128
Goat polyclonal anti-SOX2 (1:300)	R&D Systems	Cat# AF2018; RRID: AB_355110
Mouse monoclonal anti-TH (1:500)	OriGene	Cat# TA506549; RRID: AB_2623798
Rabbit polyclonal anti-TH (1:1000)	Pel-Freez Biologicals	Cat# P40101-0; RRID: AB_461064

(Continued on next page)

Continued

REAGENT or RESOURCE	SOURCE	IDENTIFIER
Sheep polyclonal anti-TH (1:800)	Pel-Freez Biologicals	Cat# P60101-0; RRID: AB_461070
Mouse monoclonal anti-VWF (1:1000)	Thermo Fisher Scientific	Cat# MA5-14029; RRID: AB_11001165
Chemicals, peptides, and recombinant proteins		
2-mercaptoethanol	Sigma-Aldrich	Cat#M6250
6-hydroxidopamine	Tocris	Cat# 2547/50
7AAD (1:5000)	Biolegend	Cat#420404
Accutase	StemCell Technologies	Cat# 07922
Ammonium Chloride (NH ₄ Cl)	Sigma-Aldric	Cat# 254134-5G
Annixin-V, FITC-conjugated (1:100)	Thermo Fisher Scientific	Cat# A13201
Annixin Binding Buffer	Thermo Fisher Scientific	Cat#V13246
Ascorbic acid	Sigma-Aldrich	Cat# A4403
B27 Supplement (50x) with VitA	Life Technologies	Cat# 17504044
B27 Supplement (50x) without VitA	Life Technologies	Cat# 12587001
Brain-derived neurotrophic factor	R&D Systems	Cat# 248-BDB
CellTrace™ Violet (1μl/10 ⁷ cells)	Thermo Fisher Scientific	Cat#C34571
CellTrace™ Calcein Violet AM (1μl/10 ⁶ cells)	Thermo Fisher Scientific	Cat#C34858
CellTracker™ Orange CMTMR Dye (1:1000)	Thermo Fisher Scientific	Cat#C2927
CHIR99021	Miltenyi Biotech	Cat# 130-103-926
Colony-stimulating factor 1	R&D Systems	Cat#216-MC
CountBright™ Absolute	Thermo Fisher Scientific	Cat#C36950
Cresyl Violet	ProSiTech	Cat#SKU: C0941-DWS
D-amphetamine sulfate	Tocris Bioscience	Cat# 2813
Diaminobenzidine	Sigma-Aldrich	Cat#D12384
DAPI (1:50000)	Sigma-Aldrich	Cat# D8417
DPX mounting media	Sigma-Aldrich	Cat#06522
Dibutyryl cAMP	Tocris Bioscience	Cat# 1141
Dulbecco's Modified Eagle Medium/ Nutrient Mixture F-12	Gibco	Cat# 11320033
DMSO	Sigma-Aldrich	Cat#D2438
Donkey Serum	Sigma-Aldrich	Cat#D9663
Ethylenediaminetetraacetic acid (EDTA) solution	Sigma-Aldrich	Cat# 03690
FcR Blocking Reagent	Miltenyi Biotec	Cat# 130-059-901
Fetal Bovine Serum	Scientifix	Cat# SKU: SFBS-AU
Fetal Calf Serum	Scientifix	Cat# SKU: SNCS-NZ
Fluoromount™ Aqueous Mounting Medium (Dako)	Sigma-Aldrich	Cat#F4680
Ficoll® Paque Plus	Sigma-Aldrich	Cat# GE17-1440-02
Fms-related tyrosine kinase 3 ligand	PeproTech	Cat# # 300-19-10UG
Ganciclovir / Cymevene	Roche	Cat# 1549922
Glacial acetic acid	Sigma-Aldrich	Cat#E6283
Glial cell line-derived neurotrophic factor	R&D Systems	Cat# 212-GD
GlutaMAX Supplement	Gibco	Cat# 35050061
Granulocyte macrophage colony-stimulating factor	Peprotech	Cat# 300-03-20UG
Hydrogen Peroxide, 30%	Thermo Fisher Scientific	Cat# H325-500
Human Serum Albumin	Sigma-Aldrich	Cat# SRP6182
Interleukin-4	Peprotech	Cat# 200-04-20UG
Interleukin-15	Peprotech	Cat# 200-15-10UG
Insulin-Transferrin-Selenium-Sodium Pyruvate	Life Technologies	Cat# 51300044
Laminin-521	StemCell Technologies	Cat# 77003
LDN193189	Tocris	Cat# 6053
Lipopolysaccharide	Sigma-Aldrich	Cat# 437628

(Continued on next page)

Continued

REAGENT or RESOURCE	SOURCE	IDENTIFIER
Matrigel	Corning	Cat#354277
Methanol	Sigma-Aldrich	Cat# 34860-1L-R
mTeSR1	StemCell Technologies	Cat# 85880
MEM alpha	Gibco	Cat# 12571063
MEM Non-Essential amino Acids (100x)	Life Technologies	Cat# 11140050
N-[N-(3,5-Difluorophenacetyl)-L-alanyl]-S-phenylglycine t-butyl ester (DAPT)	Sigma-Aldrich	Cat# D5942
N-2 Supplement (100x)	Life Technologies	Cat# 17502048
Neurobasal Medium	StemCell Technologies	Cat# 21103049
Phosphate-buffered saline ^{Mg²⁺/Ca²⁺}	Gibco	Cat# 14190250
Penicillin/Streptomycin	Gibco	Cat# 15140122
Peroxidase conjugated streptavidin ABC-HRP Kit	Vector laboratories	Cat#PK-6100
Phytohemagglutinin	Sigma-Aldrich	Cat# L8754-5MG
Potassium Bicarbonate (KHCO ₃)	Sigma-Aldrich	Cat# 237205
Propidium Iodide (1:10000)	Thermo Fisher Scientific	P1304MP
Purmorphamine	Tocris Bioscience	Cat# 4551
ReLeSR	StemCell Technologies	Cat# 05873
RNAlater®	Thermo Fisher Scientific	Cat# AM7020
RPMI-1640 Medium	Gibco	Cat# 11875119
SB431542	R&D Systems	Cat# 1614
SHH C25II	R&D Systems	Cat# 464-SH
Sodium Acetate	Ajax Finechem	Cat# AJA679-500
Sodium Pyruvate	GIBCO	Cat#11360070
Stem Cell Factor	Peprotech	Cat# 300-07-10UG
TGFβ3	Peprotech	Cat# 100-36E
Thrombopoietin	Peprotech	Cat# 300-18-10UG
Trypan blue solution	Gibco	Cat# 15250061
X-VIVO-10 media	Lonza	Cat# 216938
Y27632 (ROCK inhibitor)	Tocris Bioscience	Cat# 1254

Critical commercial assays

6Ckine/CCL21 Human ELISA Kit	Thermo Fisher Scientific	Cat# EHCL21
BD Cytometric Bead Array kit	BD Biosciences	Cat#560111, 558273, 558274, 558264
CyQUANT™ LDH Cytotoxicity Assay Kit	Thermo Fisher Scientific	Cat# C20300
MycobAlert™ Mycoplasma Detection Kit	Lonza	Cat# LT07-218
Isolate II RNA Minikit	Bioline	Cat# BIO-52072
SuperScript™ VILO™ cDNA Synthesis Kit	Invitrogen	Cat# 11754050
STEMdiff Trilineage Differentiation Kit	StemCell Technologies	Cat# 05230
PowerUp SYBR Green Master Mix kit	Applied Biosystems	Cat# 11762100

Experimental models: Cell lines

FailSafe™ H1 human embryonic stem cells	Andras Nagy Laboratory. ⁶⁰	N/A
FailSafe™ H1 8IM human embryonic stem cells	Andras Nagy Laboratory. (this paper)	N/A
NK-92®	Huntington Laboratory (from ATCC)	Cat#CRL-2408; RRID: CVCL_375
PB001.1 human pluripotent stem cells	Stem Cell Core Facility at the Murdoch Children's Research Institute (Melbourne)	hPSC reg: MCRIi001-A; RRID: CVCL_UK82

Experimental models: Organisms/strains

Mouse: BALB/c-Foxn1 ^{nu} /Arc	Animal Resources Centre	Cat# BCNU
Mouse: NOD.Cg-Prkdc ^{scid} IL2rg ^{tm1Wjl} /Sz	The Jackson Laboratory	RRID: IMSR_JAX:005557

(Continued on next page)

Continued

REAGENT or RESOURCE	SOURCE	IDENTIFIER
Mouse: Arc:Arc(S)	Animal Resources Centre	Cat# ARC(S)mouting
Rat: CBH- ^{rnu} /Arc	Animal Resources Centre	Cat# CBHNU
Oligonucleotides		
See Table S1 for list of RT-qPCR primers	N/A	N/A
Software and Algorithms		
ImageJ (Fiji) version 2.0.0	NIH	RRID: SCR_003070, https://imagej.net/Fiji
Imaris version 10.1.0	Bitplane	RRID: SCR_007370, http://www.bitplane.com/imaris/imaris
Graphpad Prism version 10.2	Graphpad	RRID: SCR_002798, https://www.graphpad.com
FlowJo version 10.9.0	Becton, Dickinson and Company	RRID: SCR_008520, https://www.flowjo.com/
Adobe Photoshop CC	Adobe	RRID: SCR_014199, https://www.adobe.com/products/photoshop.html
Adobe Illustrator CC	Adobe	RRID: SCR_010279, https://www.adobe.com/products/illustrator.html

EXPERIMENTAL MODEL AND STUDY PARTICIPANT DETAILS

Rodents

All animal procedures were conducted in agreement with the Australian National Health and Medical Research Council's published Code of Practice for the Use of Animals in Research, and approval granted by The Florey Institute of Neuroscience and Mental Health Animal Ethics committee (ID: 20-050) or Walter and Eliza Hall Institute Animal Ethics Committee as well as the University of Melbourne Human Research and Ethics Committee (ID 30812). Immune compromised adult male and female athymic nude ($n=20$, BALB/c-*Foxn1^{rnu}*/Arc), NSG ($n=12$, NOD.Cg-Prkdc^{scid} IL2rg^{tm1Wjl}/Sz; The Jackson Laboratory) and immune competent Swiss ($n=10$, Arc:Arc(S)) mice, as well as athymic nude rats ($n=20$, CBH-^{rnu}) were used in the study. Animals were group housed in individually ventilated cages, on a 12:12hr light/dark cycle with ad libitum access to food and water. Animals were grouped by gender and were test-and drug-naïve prior to commencement of the study. Littermates of the same sex were randomly assigned to experimental groups.

Humanized immune system mice were generated as previously described.⁶¹ In brief, ~1million human cord blood CD34⁺ hematopoietic stem cells (HSCs) (Lonza, 80-90% CD34⁺ purity) were thawed and rinsed gently in X-VIVO-10 media (without phenol red or gentamicin, Lonza) containing 10µg/mL DNase (Stem Cell Technologies), then centrifuged at 200g, 15min at 4°C. The supernatant was aspirated, and cells resuspended in 1mL of X-VIVO-10 media supplemented with 2% human serum albumin (Merck), 100ng/mL human TPO, 100ng/mL human Flt3L and 300ng/mL human SCF (all growth factors from Peprotech). Cells were cultured for 3 days in one well of a 24-well tissue culture plate (BD Falcon) at 37°C in a 5% CO₂ incubator. On day 3, suspension cells were pelleted by centrifugation at 200g, 15min at 4°C, then resuspended in sterile PBS supplemented with approximately 0.47mg/ml Trypan blue at approximately 3 x 10⁶ cells/mL. Care was taken to ensure the incompatibility of HLA groups between the H1 parental PSC line (used to generate the H1-FS and H1-FS-8IM PSC lines) and the cord blood, see [Figure S1E](#). The NSG pups were sub-lethally irradiated (150 cGy) between 24 and 48h after birth. Irradiation was immediately (within 2h) followed by intravenous injection of 1 x 10⁵ CD34⁺ HSCs (in a 30µL volume) into the temporal facial vein using a 50µL Gastight Hamilton syringe with 32-gauge small hub RN needle (0.375IN, 60deg, bio-strategy). Mandibular bleeds were performed at fourteen weeks of age to assess hematopoietic reconstitution by flow cytometry. Only animals with >30% human CD45⁺ reconstitution were included in the study, and mice with comparable levels of hCD45⁺ cells were stratified into groups to subsequently receive grafts of either H1-FS or H1-FS-8IM PSC-derived vmdA neural progenitors.

Human embryonic stem cells

Ethical oversight of PSC use was in accordance with NHMRC guidelines for ethical use of cell lines. The FailSafe™ H1 human embryonic stem cell line (male), expressing HSV-TK transcriptionally linked to the CDK1 gene (and subsequently referred to as the 'H1-FS' hPSC line), was cultured on Matrigel (hESC-qualified Matrix, LDEV-free, Corning, 160-220µg/mL in DMEM, Gibco™) and differentiated on Laminin-521 (0.5µg/cm², Biolamina) under xenogeneic-free culture conditions as previously described.⁶² The universal, cloaked hPSC line was engineered by overexpression of the 8 immunomodulatory human genes *PDL1*, *FASLG*, *CD200*, *CD47*, *CCL21*, *HLA-G*, *MFGE8* and *SERPINB9* into the H1-FS line using the PiggyBac and Sleeping Beauty transposon systems, as previously described²⁴ with loxP-flanked fluorescent reporters, utilised to isolate correctly targeted high transgene expressing clones, then removed from the cells using Cre recombinase-mediated excision of the loxP-flanked reporters. The resultant cell line was subsequently referred to as 'H1-FS-8IM'.

For the generation of iPSC derived macrophages and dendritic cells, the iPSC cell line PB001.1 (male, hPSC reg: MCRIi001-A; RRID:CVCL_UK82) was obtained from the Stem Cell Core Facility at the Murdoch Children's Research Institute, and cultured as described.⁶³

Immune cells

Human blood samples were collected from 3 male and female healthy donors and PBMCs isolated using Ficoll® Paque Plus (Sigma-Aldrich) and rapid centrifugation. Isolated PBMCs were frozen in media composed of 10% DMSO (Sigma-Aldrich) and 90% heat-inactivated fetal bovine serum (FBS, Scientifix). On the experimental day, PBMCs were thawed at 37°C in complete RPMI composed of RPMI-1640 media (Gibco™) with 10% FBS, 1% penicillin-streptomycin (Gibco™), 1% Sodium Pyruvate (Gibco™), 1% GlutaMAX (Gibco™).

Human NK-92® cells (an interleukin-2 dependent NK cell line derived from PBMCs of an individual with rapidly progressive non-Hodgkin's lymphoma) were cultured in flasks using MEM alpha (Gibco™) supplemented with fetal calf serum (10%, Scientifix), horse serum (10%, Thermo Fisher), myo-inositol (0.02mM, Sigma-Aldrich), Folic Acid (0.02mM, Sigma-Aldrich), Sodium Pyruvate (1%, Gibco™, Thermo Fisher Scientific), GlutaMAX (1%), IL-15 (5ng/ml, PeproTech).

METHOD DETAILS

Generation, validation and culture of H1-FS-8IM PSCs

The two human pluripotent stem cell (hPSC) lines were cultured as previously described.²⁶ Validation of pluripotency of the new H1-FS-8IM hPSC line was confirmed by immunocytochemistry, quantitative real time PCR (qPCR), trilineage differentiation and *in vivo* teratoma assay (described below). RT-qPCR was also employed to confirm and quantify the overexpression of the 8 transgenes in H1-FS-8IM PSC and vmDA neuronal cultures (at day 25 of differentiation *in vitro*, DIV25).

At defined days of differentiation, PSCs and resultant progenitors were pelleted and resuspended in RNAlater® (Thermo Fisher Scientific, USA). Total RNA was extracted using ISOLATE II RNA Minikit (Bioline, UK) according to manufacturer's specifications. The RNA was converted to cDNA using the SuperScript VILO cDNA synthesis kit (Invitrogen, USA). Quantitative PCR was performed using the PowerUp SYBR Green Master Mix kit (Applied Biosystems, USA) in an RG-6000 Rotogene system (Corbett Research, Australia). See Table S1 for full list of all primer sequences utilized in this study.

The supernatant from H1-FS PSC, H1-FS-8IM PSC, H1-FS vmDA and H1-FS-8IM vmDA (DIV25) was collected, snap-frozen and stored at -80°C. On the experimental day, the supernatant was thawed and the level of CCL21 was measured using the 6CKine/CCL21 Human ELISA Kit (Invitrogen). The experiment was repeated for three technical replicates and four independent cultures per condition.

Cultures of enzymatically-passaged PSCs were differentiated into the three main germ layers (ectoderm, endoderm and mesoderm) in monolayer culture using the STEMdiff Trilineage Differentiation Kit (StemCell Technologies). Differentiated cultures were harvested on day 5 (endoderm and mesoderm) or day 7 (ectoderm) for a total RNA extraction. Expression of mRNA of distinct germ layer differentiation marker genes after differentiation was assessed by qPCR using lineage-specific targeted markers.

Differentiation of the PSC line into vmDA neural progenitors, suitable for transplantation into PD models, was conducted as previously described.^{62,64} In brief, to initiate neural induction, cells were exposed to dual-SMAD inhibition using SB431542 (10µM, R&D Systems, days *in vitro* 0-4 inclusive, DIV0-4) and LDN193189 (200nM, Stemgent, DIV0-10) to generate neuroectodermal progenitors. Ventral patterning was achieved using Sonic hedgehog C25II (100ng/mL, R&D Systems) and Purmorphamine (PM, 2µM, Stemgent) from DIV1-6, in addition to caudalisation to a midbrain identity using the canonical WNT agonist CHIR 99021 (3µM, Miltenyi Biotech, DIV2-12). At DIV11, cells were transitioned into a Maturation media consisting of NBB27 supplemented with BDNF (20 ng/mL, R&D Systems), GDNF (20ng/mL, R&D Systems), TGFβ3 (1ng/mL, PeproTech), NOTCH inhibitor DAPT (10 µM, Sigma-Aldrich), ascorbic acid (200nM, Sigma-Aldrich) and dibutyryl-cAMP (0.05mM, Tocris Bioscience). Regional specification of the 2 cell lines into ventral midbrain progenitors was verified at DIV14 by OTX2, FOXA2 and Nestin immunochemistry, and their ability to terminally differentiate into vmDA validated by coexpression of FOXA2 and TH (Figures 1I and 1J). In preparation for transplantation, DIV19 vmDA cultures, comprising an asynchronous heterogeneous population of pre- and post-mitotic cells (see Figure S1F for H1-FS-8IM cultures, and previously reported for the H1-FS cell line²⁶) were dissociated using Accutase (Stem Cell Technologies) and resuspended at 100,000 cells/µL in maturation media supplemented with ROCK inhibitor Y27632 (10µM, Sigma-Aldrich).

For *in vitro* ablation of proliferative cells, in response to activation of the suicide gene, differentiating vmDA neural progenitors (generated from the H1-FS and cloaked H1-FS-8IM PSC lines) were treated daily with ganciclovir (GCV, 10µM, Roche) from DIV13-20. On DIV20 cells were fixed using paraformaldehyde (PFA, 4%, 10 min) and immunocytochemistry performed. For co-culture experiments, H1-FS-8IM derived vmDA progenitors were treated for 2 days with GCV (10µM) (DIV13-15), co-cultured with CellTrace™ Violet (CTV, Invitrogen) -labelled PBMC + PHA from DIV15 to DIV20, with daily addition of GCV, and PBMC proliferation assessed at DIV20, as described below.

Generation and co-culture of immune cell populations

PBMCs used to measure cell proliferation were labelled with CellTrace™ Violet (CTV, Invitrogen) according to the manufacturer's recommendations and effective labelling was confirmed on a flow cytometer. PBMCs were then resuspended in complete RPMI and plated on two different 96-well plates (one for the labelled PBMC and one for the unlabelled) containing DIV19 H1-FS or

H1-FS-8IM derived vmDA neural progenitors (1:6 ratio, 50k neurons : 300k PBMCs per well, 3 technical replicates per each PBMC donor and neuronal line, 3 biological replicates per line) with or without the addition of Phytohemagglutinin (10 μ g/ml, PHA, Sigma-Aldrich). As a control, PBMCs were plated in wells that did not contain neurons. At day 3 of the co-culture, 50 μ l of fresh media was added to each well. At day 5, CTV-labelled PBMCs were collected, washed and incubated for 30 min at 4°C in 50 μ l of FACS buffer (PBS^{Mg-/Ca-}, 2%FBS, 2mM EDTA (Sigma-Aldrich)) containing primary antibodies. The cells were then washed twice, resuspended in FACS buffer containing propidium iodide (PI, 0.1 μ g/mL, Invitrogen) and analysed using the Cytoflex S or LS (Beckman Coulter), with the 405, 488, 561, 638-nm excitation lasers coupled with 450/45, 525/40, 585/42, 610/20, 660/10, 660/20, 690/50, 780/60 emission filters. The plate containing PBMC not stained with CTV was used to measure cytokines concentration: the media from each well was collected, centrifuged and the clarified supernatant stored at -80°C.

As for the PBMC, a fraction of NK cells was labelled with CTV to assess NK cells proliferation. CTV labelled and unlabelled NK cells were plated on two different 96 well plates, on top of DIV19 vmDA neurons (1:10 ratio, 10,000 neurons:100,000 NK cells per well) and incubated for 4 hours. CTV-labelled NK cells were collected, washed with FACS buffer, resuspended in H₂O containing 10% Annexin-V buffer (Invitrogen™), Annexin-V antibody (1:100, Thermo Fisher) and PI (0.1 μ g/mL) and analysed on a Cytoflex LS. The media was collected from the 96-well plate with CTV-unlabelled NK cells, centrifuged and the supernatant stored at -80°C. The adherent cells were then fixed in the plate using paraformaldehyde (PFA, 4%, 10 min) and used for immunocytochemistry.

For primary NK cells experiments, frozen PBMC were thawed at 37°C, resuspended in complete RPMI and incubated for 30 min at 4°C in 50 μ l of FACS buffer containing primary antibodies. The cells were then washed twice, resuspended in FACS buffer containing 4',6-diamidino-2- phenylindole (DAPI, 1:50000, Sigma-Aldrich). Cell suspensions were passed through 70- μ m strainer and sorted on the BD FACSAria III (BD Bioscience, 278 USA) system with a 70 p.s.i. 70- μ m nozzle. Isolation of hCD56⁺ hCD3- DAPI- cells was achieved using the 488, 561 and 633-nm excitation lasers coupled with 510/20, 695/40, 610/20, 680/60 emission filters. Collected NK cells were centrifuged at 400g for 5 minute, counted and plated on top of day 19 H1FS or H1FS-8IM vmDA neurons that were labelled with CellTrace™ Calcein violet AM (Invitrogen™) according to manufacturer's specifications (1:10 ratio, 10k neurons : 100,000 NK cells per well). As a control, 3 wells of each neuronal cell line were only media changed and no NK cell was plated. After 4 hours of incubation, plates were and the number of Calcein⁺ vmDA neurons quantified as described below. The supernatant from each well was collected and the level of LDH measured using CyQUANT™ LDH Cytotoxicity Assay Kit (C20300, Invitrogen™), following the manufacturer's instructions.

For the generation of macrophages, the iPSC cell line PB001.1 was cultured in suspension in a 10cm non-treated Petri dishes (IWAKI) and placed on an orbital shaker (N-Biotek orbital shaker NB-T101SRC) in a humidified incubator with 5% CO₂ at 37°C. After 11 days of culture, cells could be observed detaching from the embryoid bodies, remaining in suspension in the media as non-adherent cells (which are characterized as CD45⁺ CD34⁺ myeloid progenitors). When all cells were collected and allowed to gravity settle in a 15 mL Falcon tube (Corning®), embryoid bodies pelleted in the bottom, but myeloid progenitors stayed in suspension in the supernatant, and could then be collected. The supernatant was then centrifuged (Heraeus Multifuge 1S-R) at 350g for 5 minutes to pellet the progenitors. Progenitors were then resuspended in a 10% dilution in volume of FBS and 100ng/mL of macrophage colony-stimulating factor 1 (CSF-1, R&D Systems) in RPMI-1640 media. Cells were plated in Costar® 6-well tissue-culture treated plates (Corning®) for 4-7 days in stable incubator conditions (humidified, 5% CO₂, 37°C), when cells showed morphological and molecular features (CD45⁺ CD14⁺ CD11b⁺ and Iba1⁺) displayed by macrophages. On the experimental day, macrophages were harvested using EDTA (2mM) from the 6 well plates, counted and plated on top of vmDA neurons in 48 well plates (used for FACS, 100k/well, 1:2 macrophages:neurons) or 96 well plates (used for ICC, 33.33k/well, 1:2, macrophages:neurons) in macrophages media. 24h after, new media was added with or without Lipopolysaccharide (LPS) stimulation (2ng/ml, Sigma-Aldrich). On day 2 of the co-culture, media was collected from the 96 well plates, centrifuged at 400g for 5 minutes, the supernatant stored at -80°C and the plates fixed with 4% PFA. For the 48 well plates, cells were collected using Accutase incubation at 37°C for 5 minutes. The enzyme was diluted using PBS^{Mg-/Ca-} (1:1 with Accutase), the cells washed twice with FACS buffer and incubated for 30 minutes at 4°C in 50 μ l of FACS buffer containing FC block (20 μ l/10⁷ cells, Miltenyi Biotec) and primary antibodies. Cells were then washed twice, resuspended in FACS buffer containing Propidium Iodide (1:10000). Cell suspensions were passed through 70- μ m strainer and analyzed on the BD FACSAria III (BD Bioscience, USA) system at 70 p.s.i. with a 70- μ m nozzle. Detection and isolation of CD45-FITC⁺ PI⁻ and CD45-FITC⁻ PI⁺ cells were achieved using the 488-nm and 561-nm excitation lasers coupled with 530/30 and 610/20 emission filters. See Table S2 for a list of antibodies used in all FACS-based analysis.

Human PSC derived dendritic cells (DCs) were generated from PSC cell line PB001.1 derived embryoid body spheres as described above for macrophages and previously validated elsewhere.⁶⁵ CD34⁺CD45⁺ hematopoietic progenitors emerging from embryoid bodies were collected, expanded and differentiated to DCs for 11 days in RPMI-1640 media supplemented with 10% FBS, Sodium Pyruvate (20ng/ml), GlutaMax (5ng/ml), 2-mercaptoethanol (40ng/ml, Sigma-Aldrich), fms-related tyrosine kinase 3 ligand (FLT3L, 100ng/ml, PeproTech), thrombopoietin (TPO, 20ng/ml, PeproTech), granulocyte macrophage colony-stimulating factor (5ng/ml, GM-CSF, PeproTech), interleukin IL-4 (5ng/ml, IL-4, PeproTech) and stem cell factor (SCF, 100ng/ml, PeproTech). The media was changed on day 6. On DIV11, DCs were collected using EDTA in 50 μ l of FACS buffer containing primary antibodies. Cells were then washed and resuspended in FACS buffer containing 7-AAD. Cell suspensions were passed through 70- μ m strainer and sorted on the BD FACSAria III (BD Bioscience, USA) system with a 70 p.s.i. 70- μ m nozzle. Isolation of CD11c⁺ CD1c⁺ 7AAD⁻ cells was achieved using the 488, 561 and 633-nm excitation lasers coupled with 510/20, 695/40, 610/20, 680/60 emission filters. Collected DCs were centrifuged at 400g for 5 minutes, incubated in CellTracker™ Orange CMTMR Dye (1:1000, Invitrogen) diluted in DC media (no growth factors) and incubated on the upper chamber of a transwell (50k/well; 8 μ m pore size, 24w plate, Corning)

containing DIV19 vmDA neurons (250k/well) in the lower chamber. After 16h incubation, cells in the upper chamber were discarded and migrated DCs in the lower chambers were imaged and quantified as described below. The supernatant containing DCs was then collected, spun down (5min, 500g), resuspended in FACS buffer and analysed using FlowJo Software. The results are presented as number of CMTMR⁺ live single cells events.

Surgical Procedures

All surgeries were performed under 2–5% isoflurane anaesthesia inhalation (Baxter; Deerfield, IL, USA). In mice, 1.5 µl of 6-hydroxydopamine (6-OHDA) (1.6 µg/µl free base dissolved in a solution of 0.2 mg/ml L-ascorbic acid in 0.9% w/v NaCl) was injected into the substantia nigra using a 10µl Hamilton syringe fitted with a finely pulled glass capillary at the following stereotaxic coordinates: 3.0mm posterior, 1.2mm lateral to bregma, and 4.2mm below the dura surface. Rats received unilateral injections of 6-OHDA (4µl of 3.5 µg/µl) into the medial forebrain bundle, coordinates 3.4mm posterior, and 1.3mm lateral to bregma, and 6.8mm below the dura surface.

After 6-OHDA lesioning, animals received intrastriatal grafts of vmDA progenitors derived from H1-FS or H1-FS-8IM hPSC line (100,000 cells in 1µl). Stereotaxic coordinates for mice were: 0.5mm anterior, 2.5mm lateral to bregma, 4mm below the dura surface; rats: 0.5mm anterior, 2.5mm lateral to Bregma and 4.0mm below the dura surface.

A subset of athymic nude mice (n=8) received daily intraperitoneal (i.p.) injections of GCV (50 mg/kg) from 8–9 weeks after transplantation, to activate the HSV-TK suicide gene, ablating proliferating cells within the grafts.

Behavioural Testing

Four weeks after lesioning in rats, unilateral DA function was assessed using the amphetamine-induced rotation test, with re-testing performed at various intervals following transplantation. In brief, net rotations over 60 minutes were analysed 10 minutes after intra-peritoneal injection of D-amphetamine sulfate (5mg/kg; Tocris Bioscience). Upon completion of initial testing 4 weeks post-lesioning, animals displaying a functional deficit (>300 rotations in 60 min) were ranked in order of the percentage rotational asymmetry and evenly distributed across the three treatment groups: (i) Lesion only, (ii) Lesion + H1-FS graft, (i) Lesion + H1-FS-8IM graft. To assess functional integration of the transplanted cells, rats were re-tested at 16 and 20 weeks after grafting.

Tissue isolation

At 8 weeks post-transplantation, Hu-NSG-SGM3-CD34 mice were anaesthetised with 2–5% isoflurane, the cisterna magna exposed and punctured using a finely pulled glass capillary. The clear cerebrospinal fluid (CSF) was collected, snap-frozen in dry ice and stored at -80°C. Unclear CSF was discarded. At this time, animals received a lethal dose of sodium pentobarbitone (100 mg/kg), spleen and cervical lymph nodes were isolated (see below), and mice subsequently transcardially perfused with warmed tyrode buffer followed by 4% PFA. Brains were isolated and snap frozen for histochemical assessment (see below).

For *in vivo* assessments of grafts in immune competent swiss mice, as well as immune compromised athymic nude mice and rats, animals were killed by an overdose of sodium pentobarbitone (100 mg/kg) at 4 weeks (teratoma assessment), 8–9 weeks (mice) or 20 weeks (rats), followed by transcardial perfusion with warmed tyrode buffer followed by 4% PFA.

Immunophenotyping

Flow cytometry was used to immunophenotype humanised mice. All centrifuge spins were performed at 500g for 5 min at 4°C. Briefly, blood was collected from the mice submandibular vein into EDTA tubes (Interpath) and kept on ice. 25µl of blood was used for flow cytometry, the remaining volume was centrifuged, the plasma snap-frozen in dry ice and stored at -80°C. Cervical lymph nodes (LN) and spleen were weighted, processed into single cell suspension by mashing through a 70µm cell strainer into a solution of complete RPMI. This single cell suspension was centrifuged at 500g for 5 min. The spleen samples were resuspended in 2ml of ACK Red Cell Lysis buffer (154 mM NH₄Cl, 10 mM KHCO₃ and 100 mM EDTA, pH 7.3) for 3 minutes, FACS buffer was added and the sample centrifuged. Spleen and lymph nodes were then resuspended in 1ml (spleen) or 500µl (lymph nodes) of FACS buffer. 25 µL of each sample was transferred into a 96-well U-bottom plate. For the blood, erythrocytes were removed by resuspending cells in ice-cold ACK buffer for 3–4 min until the blood was clear. ACK lysis was repeated twice before cells were washed with PBS-FCS. All samples are stained with 30µl of FACS buffer containing primary antibodies for 30 min at 4°C. Cells were then resuspended in 200µl FACS buffer containing 5000 Counting Beads (5µl of stock beads + 195µl 2% FCS/PBS per sample, CountBright™ Absolute, Invitrogen). Samples were analysed using a LSRII Fortessa X20 (BD Biosciences) or Aurora (Cytek). All data were analysed using FlowJo Software (10.9.0 © Becton Dickinson & Company (BD) 2006–2023). Representative FACS plots, illustrating gating strategies for each of the defined populations, are shown in [Figure S6](#).

Human interferon-gamma (IFN-γ), tumour necrosis factor-alpha (TNF-α) and interleukin-10 (IL-10) were measures from cell culture supernatant, plasma and CSF samples using the BD Biosciences Cytometric Bead Array kit (560111, 558273, 558274, 558264, BD Life Sciences) following the manufacturer's recommendations. For *in vitro* assays, three wells (technical replicates) per culture condition were analysed and repeated across three independent experiments.

Tissue Processing and Immunohistochemistry

In vitro cultures were fixed using paraformaldehyde (PFA, 4%, 10 min) prior to immunocytochemistry. Brains were cryosectioned (40µm, 12 series) on a freezing microtome and immunohistochemistry was performed on free-floating brain sections as previously

described.²⁶ Primary antibodies and dilutions are shown in **Table S3**. Secondary antibodies for i) direct detection included Alexa Fluor 488 or 647 (Jackson ImmunoResearch) or DyLight 550 (Abcam) conjugated donkey anti-goat, anti-rat, anti-mouse, anti-rabbit, and anti-sheep, and ii) chromogenic detection of antibody- DAB complex (biotin-conjugated donkey anti-rabbit, Jackson ImmunoResearch) were used at a dilution of 1:200, 2 h. For chromogenic staining, secondary antibodies incubation was followed by peroxidase conjugated streptavidin (2 hours, Vectastain ABC kit, Vector laboratories) and incubation with DAB (0.5 mg/ml, 2 min), which was precipitated by addition of 1% [w/v] H₂O₂. Fluorescently labelled sections were cover-slipped with fluorescent mounting media (Dako); Cresyl and chromogenic labelled sections were dehydrated in alcohol and xylene and cover-slipped with DePeX mounting media (BDH Chemicals, UK) on gelatinized slides. Total cells *in vitro* and *in vivo* were visualised with 4',6-diamidino-2- phenylindole (DAPI, 2µg/mL, Sigma-Aldrich).

To reveal gross teratoma morphology (to confirm pluripotency of the new cloaked line), free-floating tissue sections containing the graft/tumor were immersed for 2 minutes in Cresyl violet solution made of 0.5% [w/v] Cresyl Violet (ProSiTech), 0.06 M sodium acetate (Ajax Finechem), 2.5% [v/v] glacial acetic acid (Merck) in dH₂O. Cresyl labelled sections were dehydrated in alcohol and xylene, mounted on gelatinized slides and cover-slipped with DePeX mounting media.

QUANTIFICATION AND STATISTICAL ANALYSIS

Note, all behavior testing and histological assessments were performed with the researcher blinded to the experimental group.

Brightfield and darkfield images of chromogenic staining were captured using a Leica DM6000 microscope. Fluorescent images were captured on a Zeiss Axio Observer Z.1, Invitrogen EVOS M5000, Zeiss LSM 780 or Zeiss CellDiscoverer 7 microscope.

For *in vitro* quantification of pluripotency, vmDA fate specification, neural maturation, immune cells, and apoptosis, images captured at 20x magnification were used to quantify the total number of DAPI, OCT4, SOX2, NANOG, OTX2, FOXA2, TH, CD45, MAP2, NEUN and Cleaved-Caspase3 immunolabelled cells. Quantification of viable (non-pyknotic) DAPI, pyknotic and immunolabelled cells was performed across three fields of view (FOV) per well, with three wells (technical replicates) per culture condition and repeated across three independent experiments. To quantify the immune response of CD45⁺ macrophages to H1-FS or H1-FS-8IM derived neurons, three FOV per well with three wells (technical replicates) per culture condition were imaged and the area covered by CD45⁺ immunoreactive pixels was expressed as a percentage of the total pixels. For DCs quantification, three FOV per well per culture condition were imaged and the number of CMTMR⁺ cells were counted using Fiji ImageJ – Analyse particles function.

Macrophages phagocytosis was quantified using Imaris 10.1.0 (Bitplane) in a three-dimensional (3D) tissue volume acquired by confocal microscopy at three fields of view per well with a Zeiss Celldiscoverer 7 confocal microscope (Carl Zeiss, Germany), using a Plan-Apochromat 20x/0.7 objective paired with a 0.5x Tubelens, 3 wells/condition. Images were then processed using the Zeiss LSM processing function. For phagocytosis quantification, briefly, 3D surface reconstruction was created in the MAP2⁺ and CD45⁺ channels. A shortest distance surface-surface filter set to <0 µm was applied to identify and isolate the number of CD45⁺ macrophages that contained MAP2⁺ cells. The colocalised MAP2⁺ and CD45⁺ surfaces were then reconstructed in a separate surface for analysis.

To quantify dendritic cells migration and number of Calcein⁺ vmDA neurons upon co-culture with NK cells, 3 fields of view / well were imaged on an Invitrogen EVOS M5000 Imaging System. The number of CMTMR⁺ DCs and Calcein⁺ vmDA neurons were counted using Fiji ImageJ – Analyse particles function.

Human-specific PSA-NCAM and human nuclear antigen (HNA⁺) immunolabelling was used to delineate the graft boundaries and estimate graft volume according to Cavalieri's principle. For *in vivo* cell counting, all TH⁺ cells were counted throughout the entire graft from a 1/12 series. The fraction of GIRK2⁺ and CALB⁺ expressing cells was quantified by examining all TH⁺ cells across three fluorescent immuno-labelled sections while HNA⁺ and NeuN⁺ cells were counted in 3 fields of view (20x)/ section from 3 graft sections/brain. Total numbers estimated using density and graft volume.

TH⁺ fibre density was measured as optical density in single fields of view (20x) of 1/12 series of chromogenic immunohistochemistry for TH as previously described.⁶⁶ Measurements spanned 5 sections from 1.70mm anterior to -0.80mm posterior to Bregma, sampling the dorsolateral striatum (AP: 0.20, ML: -3.8 and DV: -3.9).

The immunological response of the host brain to the grafted cells was assessed at predetermined sites lateral to the graft-host border (delineated according to HNA labelling), as indicated in **Figure 3G**. The density of GFAP⁺ astrocytes or Iba1⁺ microglia was calculated as area covered by GFAP/Iba1 immunoreactivity pixels expressed as a % of the total pixels in the H1-FS/H1-FS-8IM transplanted brain. Microglial reactivity was assessed as the proportion of Iba1⁺ cells showing stellate (healthy) versus ameboid-like morphology (reduced processes). For quantitative purposes, confocal captured images (63X) showing Iba1⁺ labelling were thresholded using the auto local thresholding algorithm, Phansalkar, and cells filtered as objects ranging 10-600 µm². Individual cells were skeletonised and skeleton analysis was conducted as expressed as endpoints/cells (ie ramifications/cells).

All data are presented as mean ± SEM, except where stated. All data were tested for normality (Shapiro-Wilk test) and statistical analyses performed (Mann-Whitney U-test for non-normal distributed and Student's *t*-test for normal distributed data) are stated in the figure legends. All statistical analyses were performed using GraphPad Prism version 10.2 (RRID: SCR_002798, <https://www.graphpad.com>) and alpha levels of *p* < 0.05 were considered significant (**p* < 0.05, ***p* < 0.01, ****p* < 0.001, *****p* < 0.0001).